Journal of Materials Chemistry C

ROYAL SOCIETY OF CHEMISTRY

REVIEW

View Article Online
View Journal

Cite this: DOI: 10.1039/d2tc00318j

Heat-shedding with photonic structures: radiative cooling and its potential

Se-Yeon Heo, [a] Gil Ju Lee †*[b] and Young Min Song †*[a]

Radiative cooling, which is based on radiative heat exchange between the universe and Earth, can provide a passive and renewable route to reducing energy consumption. Radiative cooling was historically limited to nighttime applications owing to a lack of solar reflectivity. However, recent advances in photonics have facilitated the realization of multi-spectral features, such as near-unity solar spectrum reflection and atmospheric transparent window thermal emission for daytime radiative cooling. This review highlights recent progress and continued efforts in photonic radiators for daytime radiative cooling. First, we provide an overview of the fundamentals of passive radiative cooling, using the universe as a heat sink. Then, we assess advances in radiators, from traditional applications of buildings and textiles, to newly pioneered fields such as vehicles, wearables, solar cells, thermoelectric generators, and radiative condensers. Each application includes the requirements in terms of materials and optical/mechanical/thermal designs. Next, we discuss self-adaptive radiative thermostats for considering seasonal climate variation. Subsequently, challenges from fundamental limitations in passive radiative cooling and emerging issues with technical evolution are discussed, along with potential solution strategies.

Received 21st January 2022,
Accepted 9th June 2022

DOI: 10.1039/d2tc00318j

rsc.li/materials-c

1. Introduction

In thermodynamics, the universe acts as a blackbody at a temperature of a few absolute degrees. If shielded from sunlight, an object with a finite temperature outside the atmosphere will spontaneously cool by emitting thermal radiation, while the thermal energy received from outer space is negligible.[1] However, if the object is placed on the Earth, the phenomenon is significantly influenced by the atmosphere.[2] The atmosphere transfers heat energy to the object in three ways. First, solar radiation scatters towards the object at a wavelength smaller than 4 μm. Second, heat is provided through air as a medium *via* conduction and convection (non-radiative heat exchange). Third, the atmosphere itself emits thermal radiation to the object.[1,3] The net energy flux of the object is a combination of the incoming heat absorption from the sun and atmosphere, outgoing thermal radiation, and heat lost through conduction and convection (Fig. 1a).

The phenomenon, labeled passive radiative cooling, has been recognized since ancient times;[4] to the knowledge of the authors, the first scientific discussion was made in 1828 by Arago[5] who wrote: ''If we place in the open air, in a calm and serene night, small masses of grass, cotton, sodas, or any other filamentous substance, we find, after a certain time, that their temperature is 6, 7 and even 8 Celsius below the ambient temperature.'' The key to radiative cooling is to understand the spectral emission of the atmosphere. The thermal radiation of the atmosphere is weak in the wavelength range of 8–13 μm. Therefore, the blackbody radiation emitted by a surface exposed to the sky is not balanced by an equal amount of counter-radiation. Moreover, it can be cooled to a temperature below the ambient temperature.[3]

The early development of radiative coolers took inspiration from nature, such as the formation of frost and dew on plants. In addition, animals such as the Saharan silver ants[6] and white beetles[7] passively cool themselves to survive under extreme temperatures. However, until recently, radiative cooling was restricted to nighttime from a relatively limited selection of bulk materials. Although solar-reflecting materials have been reported, daytime cooling to below ambient temperature has not been achieved with natural materials because solar absorbance exceeds the energy emitted from the object.[8] With advancement in nano- and micro-photonic technologies, natural materials were gradually replaced by synthetic compounds or polymers that enabled achieving a surface temperature below ambient temperature under direct sunlight. Following the first report of a daytime radiative cooler with a photonic

[a] School of Electrical Engineering and Computer Science (EECS), Gwangju Institute of Science and Technology (GIST), 61005, Republic of Korea. E-mail: ymsong@gist.ac.kr
[b] Department of Electronics Engineering, Pusan National University, 46241, Republic of Korea. E-mail: gjlee0414@pusan.ac.kr
† Gil Ju Lee and Young Min Song are co-corresponding authors.

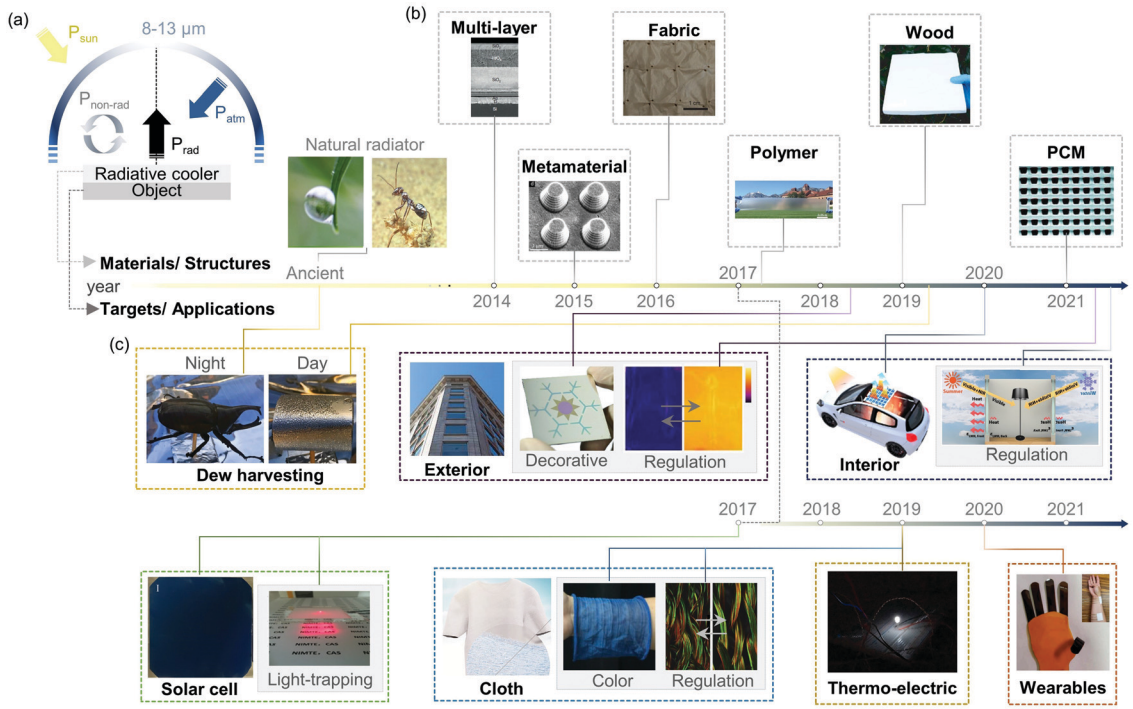

Fig. 1 Summary of the mechanism, material, and application of radiative cooling in history. (a) Radiative heat transfer between a passive radiative cooler and the universe. (b) Timeline of radiative cooling materials and structures, from natural radiators such as leaves (reproduced with permission. Copyright © Create Commons Zero. MaxPixel.) and the Sahara silver ant (reproduced with permission.[6] Copyright © 2015. AAAS), to artificial radiative cooling structures, including multi-layer structure (reproduced with permission.[9] Copyright © 2014. Springer Nature), metamaterial (reproduced with permission.[10] Copyright © 2015. John Wiley & Sons, Inc.), fabric (reproduced with permission.[11] Copyright © 2016. AAAS), polymer (reproduced with permission.[12] Copyright © 2017. AAAS), and natural wood (reproduced with permission.[13] Copyright © 2019. AAAS). (c) Timeline of targets and applications of radiative cooling. The initial demonstration of the application is indicated along with additional functions. For instance, the radiative cooler which is used for both cooling and decoration is indicated next to the building figure. Applications include day (reproduced with permission.[14] Copyright © 2021. National Academy of Sciences) and night dew harvesting, decorative (reproduced with permission. Copyright © Create Commons Zero. NegativeSpace), exterior building cooling (reproduced with permission.[16] Copyright © 2018. John Wiley & Sons, Inc.), thermoregulating cooler (reproduced with permission.[75] Copyright © 2021. AAAS), enclosure cooling (reproduced with permission.[17] Copyright © 2020. AAAS) and thermo-regulation window (reproduced with permission.[74] Copyright © 2021. AAAS), solar cell cooling (reproduced with permission.[20] Copyright © 2017. American Chemical Society) and light trapping radiative cooler (reproduced with permission.[148] Copyright © 2017. John Wiley & Sons, Inc.), cloth (reproduced with permission.[107] Copyright © 2019. AAAS), colored textile (reproduced with permission.[96] Copyright © 2019. Cell Press), thermo-regulating textile (reproduced with permission.[188] Copyright © 2019. AAAS), thermoelectric generation (reproduced with permission.[21] Copyright © 2019. Cell Press), and wearable device cooling (reproduced with permission.[127] Copyright © 2020. National Academy of Sciences).

design in 2014,[9] scientists and engineers have endeavored to develop more robust materials for effective cooling during day- and nighttime. The progression of suitable radiative cooler materials is illustrated in Fig. 1b; in 2015, an array of shaped conical metamaterial pillars achieved near-ideal emission within the 8–13 μm wavelength range;[10] in 2016, a wearable textile that promotes effective radiative cooling was demonstrated;[11] in 2017, polymer-based radiators with large scalability was achieved;[12] in 2019, engineered cooling wood that endows the natural structure with stronger mechanical strength was realized.[13] At present, passive radiative cooling materials with an optimized structure type and design serve in a variety of strategic fields.

Radiative cooling technology can be integrated with building, transportation, energy harvesting, and wearables for outdoor activities (Fig. 1c). From the moment that humanity ceased to depend on nighttime radiative cooling, the range of applications has continuously expanded. Daytime dew harvesting was achieved only a few years ago. Distinct from darkling beetles that use nighttime radiative cooling to collect water in the Namib desert, radiative condensers that operate for 24 h have been demonstrated for passive water extraction and purification technologies.[14] Applications in building cooling has significant potential for next-generation renewable energy-efficient temperature regulation.[15] Radiative cooling technology continues to evolve as the demand for further functionality grows. For example, a material that is both cooling and decorative has been demonstrated.[16] Beyond building cooling, a bi-directional radiative cooler that targets thermally enclosed spaces has also been reported.[17] Clothing, food, and housing are essential elements of human life.[18] Radiative textiles are directly related to comfort and have been demonstrated to effectively regulate temperature.[11] Flexible radiative cooling materials that possess enhanced mechanical properties allow for the development of wearable devices.[19] Furthermore, radiative coolers can lower the temperature of solar panels, preventing thermal degradation,[20] and contribute to direct energy production in thermoelectric devices.[21]

Passive radiative cooling has been discovered, observed, used, and examined over a long period of time. Various reports have offered thoughtful reviews of historic radiative coolers.[1,8,15,22–25] However, few comprehensively highlight the challenges, potential solutions, and prospects of radiative coolers from a combined commercial and academic point of view. Moreover, the abundant applications of this innovative field warrant an updated survey. Therefore, by compiling the knowledge and experience gained from pioneering studies, the authors of this review wish to contribute to the further advancement of the field. Herein, we summarize the state-of-the-art of radiative coolers, encompassing advanced materials, structures, applications, and underlying mechanisms. The review begins with a basic overview of the fundamental principles of radiative cooling. Specifically, we compare the power balance equation and two classic types of radiative coolers. The third section introduces salient applications, including a detailed discussion of the key design principles for each. Photonic approaches, including film-, microstructure-, and particle-based thermal emitters, are also discussed. In addition, thermoregulatory materials that adjust the spectral performance under visible and infrared radiation are presented. Although innovative concepts have arisen from the research laboratory, radiative cooling technology is only now beginning to be commercialized,[26–30] and there is remaining uncertainty regarding their practical application. In the final section, the challenges and perspectives for the real-world deployment of these systems are summarized.

2. Fundamental and physical model

The heat emitted from a radiative cooler escapes to outer space through the highly transparent wavelength range between ~8 and ~13 μm of Earth's atmosphere (*i.e.*, the atmospheric transparent window, ATW). For an emitter at temperature T with a spectral and angular emissivity $\varepsilon(\lambda, \theta)$, the net radiative cooling power $P_{\text{cool}}(T)$ is composed of four power terms and defined as:

$$P_{\text{cool}}(T) = P_{\text{rad}}(T) - P_{\text{atm}}(T_{\text{amb}}) - P_{\text{sun}} - P_{\text{cond+conv}} \quad (1)$$

where P_{rad} denotes the radiated power of the radiator, P_{atm} is the radiated power from the atmosphere absorbed by the radiator, P_{sun} refers to the absorbed solar energy, and $P_{\text{cond+conv}}$ denotes convective and conductive heat exchange between the radiator and the surroundings. T_{amb} is the temperature of ambient air. The radiator is in a steady-state when P_{cool} is zero. While in a steady-state, if the temperature of the radiator is lower than that of ambient air (*i.e.*, $T < T_{\text{amb}}$), the radiator is in cooling mode, and, if $T > T_{\text{amb}}$, the radiator is in heating mode. The four power terms are calculated as follows:

$$P_{\text{rad}}(T) = \int_0^{2\pi}\int_0^{\frac{\pi}{2}}\int_0^{\infty} I_{\text{BB}}(T,\lambda)\varepsilon(\lambda,\theta)\cos(\theta)\sin(\theta)\mathrm{d}\lambda\mathrm{d}\theta\mathrm{d}\phi \quad (2)$$

$$P_{\text{atm}}(T_{\text{amt}}) = \int_0^{2\pi}\int_0^{\pi/2}\int_0^{\infty} I_{\text{BB}}(T_{\text{amb}},\lambda)\varepsilon(\lambda,\theta)\varepsilon_{\text{amb}}(\lambda,\theta) \times \cos(\theta)\sin(\theta)\mathrm{d}\lambda\mathrm{d}\theta\mathrm{d}\phi \quad (3)$$

$$P_{\text{sun}} = \int_0^{\infty} I_{\text{AM1.5G}}(\lambda)\varepsilon(\lambda,\theta)\mathrm{d}\lambda \quad (4)$$

$$P_{\text{cond+conv}} = h_{\text{c}}(T - T_{\text{ambient}}) \quad (5)$$

Here, $I_{\text{BB}} = \left(2hc^2/\lambda^5\right)\Big/\left[\mathrm{e}^{\frac{hc}{\lambda k_{\text{B}}T}} - 1\right]$ is the spectral radiance of a blackbody at temperature T, where h, c, k_{B}, λ, and h_{c} are the Planck constant, velocity of light, Boltzmann constant, wavelength, and non-radiative heat exchange coefficient, respectively. The atmospheric emissivity is given by $\varepsilon_{\text{amb}}(\lambda, \theta) = 1 - t(\lambda)^{1/\cos(\theta)}$, where t is the transmittance of the atmosphere in the zenith direction.

A radiative cooling device can be classified as either a selective or broadband emitter depending on its spectral emissivity profiles. A selective emitter has unity emissivity only in the ATW (8–13 μm) and zero elsewhere. The emissivity profile of a broadband emitter resembles that of a blackbody, except for the solar spectral range from 0 to 2.5 μm. Below-ambient radiative cooling materials aim to have low steady-state temperatures, where a selective emitter is superior. This is because the low selective emission profile outside the 8–13 μm range ensures minimal radiative heat exchange with the atmosphere *via* other infrared wavelengths. In comparison, above-ambient cooling aims to provide maximal cooling power, where a broadband emitter is superior. Different types of radiative cooling can be used depending on the working temperature of the system. A broadband emitter emits more radiative power at an operating temperature higher than ambient than what it receives at ambient temperature.[8] For example, below-ambient cooling is widely used for the thermal management of buildings, while the broadband emitter is more suitable for dissipating heat in solar cell cooling, because the elevated working temperature and high atmospheric transmittance are ideal conditions for maximizing the cooling power.[31] Therefore, it is essential to choose a cooling strategy that is appropriate to target applications.

The electromagnetic spectrum can roughly be divided into six regions concerning spectral engineering in radiative cooling, as shown in Fig. 2 The solar spectrum (0.28–4 μm) has wavelength ranges between 0.28–0.4 μm (ultra-violet, UV), 0.4–0.8 μm (visible, Vis.), 0.8–1.1 μm (near-infrared, NIR), and 1.1–4 μm (mid-infrared, MIR), which dominates incoming solar radiation. The wavelength ranges between 8–13 μm is called the ATW of the long-wave infrared region (4–13 μm, LWIR), for which the atmosphere is highly transparent and radiation from the cooler can transfer heat to the outer space. Wavelengths in the ranges 4–8 μm (mid-wave infrared, MWIR) and beyond 13 μm (far-infrared, FIR) dominate the incoming atmospheric thermal radiation. By adjusting light–matter interaction characteristics in a specific range (*i.e.*, reflection, R; transmission, T; or absorption, A), the material with optimized radiative cooling

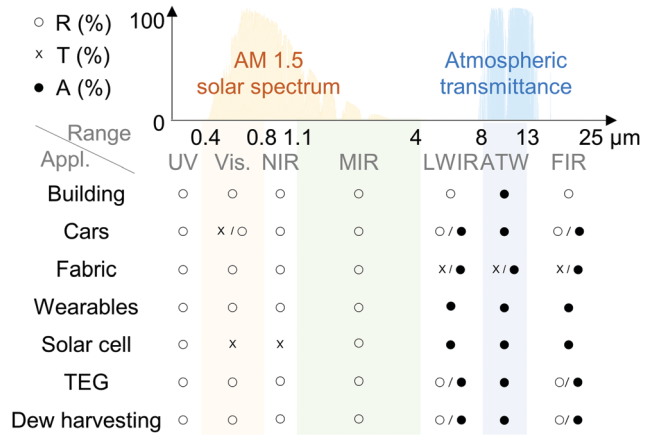

Fig. 2 Desired reflectivity (*R*), transmission (*T*), and absorptivity (*A*) characteristics for radiative cooling applications. The spectrum is divided into six ranges: the ultra-violet (UV, 0.01–0.4 μm), visible (Vis., 0.4–0.8 μm), near-infrared (NIR, 0.8–1.1 μm), mid-infrared (MIR, 1.1–4 μm), long-wave-infrared (LWIR, 4–8 μm), atmospheric window (ATW, 8–13 μm), and far-infrared (FIR, 13–25 μm). TEG = thermoelectric generator.

effects can be selected for each application (Fig. 2). For instance, the materials for solar cell applications should exhibit strong absorption from LWIR and FIR radiation, whereas high transparency is required in the Vis-NIR range.[32] On the other hand, a radiative cooler appropriate for wearable devices should exhibit high reflectance in the entire solar spectrum and strong thermal emission from LWIR and FIR radiation.[19]

The following sections summarize radiative cooling materials/structures and their design principles in key applications, such as building, car, fabric, wearable device, solar cell, thermoelectric generation, and dew harvesting technology. It also includes devices with thermostat properties that can regulate dynamic IR radiation.

3. Applications

3.1 Large-scale facilities: buildings and enclosures

3.1.1 Radiative cooling on building exteriors. Cooling accounts for approximately 12% primary energy consumption of a building and radiative cooling has been considered to improve energy-efficiency.[15,33–37] For building applications, the radiative cooler needs to have high reflectance in the solar spectrum and strong thermal emission in the ATW range (Fig. 3a). The material can be used to cover the building exteriors such as roof[38,39] and wall[34,40] in types of tiles, paints, or coatings. It has been reported that a radiative cooling roof doubles the energy savings provided by typical white roofs.[13] According to the operation model of the cooling process, the integration of radiative cooling with the building can be largely divided into air-based, water-based, and hybrid radiative cooling systems (Fig. 3a). The following sections present overviews of the three typical systems for radiative cooling of buildings.

Air-based radiative cooling systems. Air-based systems utilize air as the heat-exchange medium. The air is flown beneath the

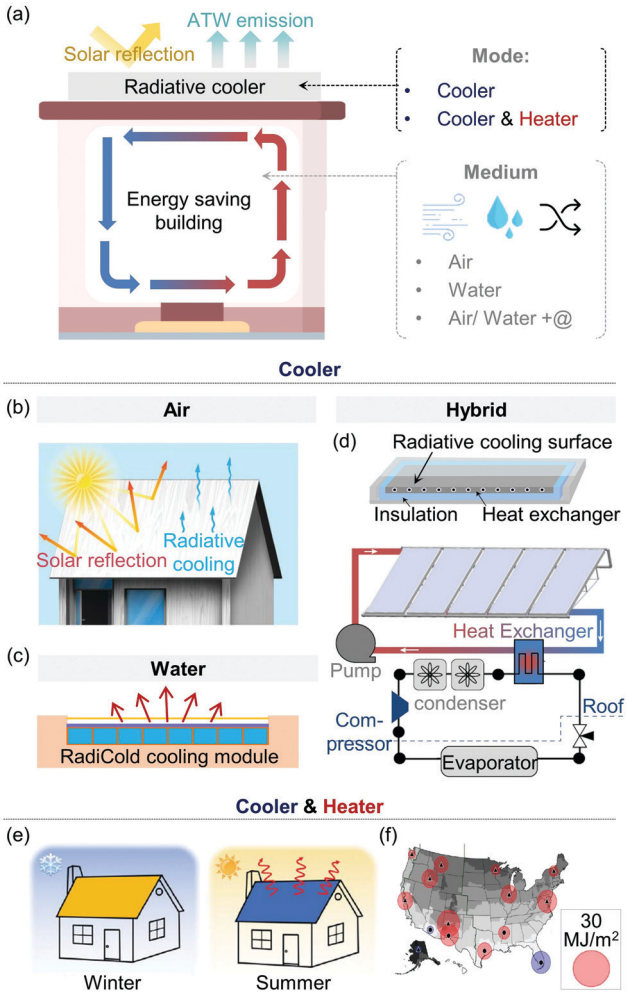

Fig. 3 Radiative cooling for building exterior. (a) A schematic for a passive radiative cooling system in buildings. (b) Model of air-based radiative cooling system on roofs and external walls of buildings. Reproduced with permission.[13] Copyright © 2019. AAAS (c) Water-based radiative cooling system. Reproduced with permission.[57] Copyright © 2019. Cell Press (d) Schematic of hybrid radiative cooling system (air-cooled vapor-compression) integrated for buildings. Reproduced with permission.[63] Copyright © 2017. Springer Nature (e) Schematics of temperature-adaptive radiative coating for temperature management when used as a household roof coating. Reproduced with permission.[75] Copyright © 2021. AAAS (f) Simulation for potential space conditioning energy savings per unit roof area attainable by using temperature-adaptive radiative coatings. Reproduced with permission.[75] Copyright © 2021. AAAS.

surface of the exterior-mounted radiator to provide instantaneous cooling. Driven by a fan or natural processes due to the buoyancy effect, continuous air flow maintains the heat transfer process between the environment and the radiator.[41] Air-based radiative cooling systems are relatively inexpensive and straightforward to install.[42] Due to its special advantages and spectral requirements (*i.e.*, high solar reflection and strong IR-emission), most daytime radiative coolers can be applied for this system. Several studies have demonstrated effective radiative cooling and energy saving in buildings.[43–46] Raman *et al.* fabricated cooling material consisting of seven layers of HfO_2 and SiO_2, which reflects 97% of incident solar radiation while strongly emitting heat in the ATW

range.[9] Li *et al.* engineered structural cooling wood composed of cellulose nanofibers.[13] The fibers functioned as randomized scattering elements for intense broadband reflection and an average of 96% solar reflectance was achieved. Simultaneously, molecular vibration and stretching of cellulose in the cooling wood result in a LWIR-FIR emissivity that is close to unity. The emissivity characteristics also showed negligible angle dependency from 0° to 60°, which is over 90% in the ATW. The structural cooling wood was reported to contribute 20–60% of energy-savings when applied to the building exterior (Fig. 3b).[13] In 2017, Zhai *et al.* compared a glass-polymer hybrid metamaterial roof[12] and a regular gray-colored shingle roof in Laramie, Wyoming, USA.[15] The maximum temperature differences at the roof surface and indoors were 28.6 and 11.2 °C for the metamaterial and shingle roofs, respectively, which could save as much as 91 kW h $(m^2\ year)^{-1}$ of cooling electricity. A radiative air-cooling system installed at an Indian multinational company achieved 40% higher energy efficiency than conventional building insulation.[47] However, there are some challenges in air-based systems associated with the relatively weak air circulation induced by natural forces. Therefore, a narrow air channel with a large surface area is required for the radiator to maximize thermal contact with the air, limiting further applications.[48]

Water-based radiative cooling systems. The water-based radiative cooling system utilizes water as a heat-transfer medium. These systems can be applied more effectively than an air-based system because of easier flow regulation and the higher heat capacity of water. The average net cooling power of water-based systems is 40–80 W m^{-2},[2,49,50] which is 10–60 W m^{-2} higher than that of the air-based systems.[50,51] Water-based cooling systems are further categorized into two operating modes, namely open or close systems.[51,52] In the open system, water serves as an *in situ* coolant that dissipates heat to the surroundings *via* radiation and evaporation.[53] A roof pond is one of the prevailing examples of the open water-based system.[54–56] Close water-based systems, on the other hand, consists of pipes filled with water. Zhao *et al.* developed the so-called RadiCold water-cooling module, as shown in Fig. 3c.[57] The module achieved 10.6 °C cooling and kW-scale heat dissipation power under direct sunlight. The suggested system is composed of multiple cooling modules and pipes. By replacing warm water from the mainstream with cold water, the system achieves continuous cooling from each unit of the cooling module. There are also key issues associated with the performance of a close water-based system that was used in recent projects at Bangkok airport in Thailand and Xi'an airport in China. It was reported that water-based radiative cooling was insufficient to cool large-space buildings during high exposure to the sun.[58] Therefore, the water-based systems can be further improved by integration with other energy systems.

Hybrid radiative cooling systems. Air- and water-based systems are single units whose cooling relies only on the spectral radiance of the medium. These systems are completely passive, achieving a relatively low cooling power compared to that of an active cooler. A hybrid system, which combines a radiative cooling system with other energy units, offers more energy-efficient cooling. Previous studies have explored various types of hybrid systems, such as integration of the radiative cooling with a fan or pump to solve the problem of thermal accumulation,[52,59] with desiccant systems to enhance the cooling performance,[60,61] with an active cooling unit to improve efficiency,[62,63] with a solar collector to realize daytime solar heating and nighttime radiative cooling,[60,64–68] with photovoltaic (PV)-thermal panels to harvest both electricity and cooling energy and heating in day, and cooling at night,[69–72] and with a phase-change material (PCM) for real-world thermal management.[73–75] Ventilation plays a key role in maintaining indoor air quality and thermal comfort.[76] With the support of a radiative cooler, the temperature of ventilated air can be further reduced.[77] Recent advances in daytime passive radiative cooling offers overall efficiency improvements. Goldstein *et al.* integrated a radiative water-cooling system with the air conditioning unit of an office building.[63] The cooling panel was able to cool water up to 5 °C below the ambient air temperature, corresponding to a heat rejection flux of up to 70 W m^{-2}. The cooled water from the panel was then used to precool the refrigerant of the air conditioning unit through a heat exchanger, as shown in Fig. 3d. The system reduced the cooling energy consumption of the building by 21%.

At present, in light of rapid seasonal climate variation, there is an enhanced need for new thermal management methods. To address this challenge, PV conversion, photothermal conversion, and radiative cooling systems were integrated. In this new hybrid system, photons with energies exceeding the band-gap of the PV material were partially converted to electricity. The remaining energy is used as heating power, while the radiative cooler offers space cooling of the building.[70,78] Contemporary material characterization and modeling tools allow the realization of completely passive all-season household thermal regulation. Tang *et al.* experimentally demonstrated a self-adaptive radiative coating by combining a daytime radiative cooler and the metal-insulator PCM WVO_2 (Fig. 3e).[75] The fabricated layer automatically switched the emittance from 0.20 for ambient temperatures lower than 15 °C to 0.90 for temperatures above 30 °C, which should achieve energy savings in most climate conditions (Fig. 3f). Additional applications of radiative self-adaptation are discussed in more detail in Section 3.5.

3.1.2 Thermally enclosed spaces: automobiles and greenhouses. Although the radiative cooling structure has been thoroughly explored, inner space cooling remains challenging. There is a high demand for a cooling solution for enclosed spaces where very high temperatures can develop. For instance, the temperature of an automobile parked under direct sunlight can rise to 60–82 °C when the ambient temperature is only 21 °C.[79] This is because car windows are transparent to incoming solar radiation while opaque to outgoing long-wave thermal radiation, which is well-known as the greenhouse effect. As a result, heat accumulates in a car, which can cause heat stroke and hyperthermia in the occupants, especially children.[80] The integration of passive radiative cooling with active cooling can potentially alleviate these problems. However, as discussed in Section 3.1.1 (Hybrid radiative cooling systems), this might incur

additional energy requirements and raise costs. Accordingly, there are ongoing efforts to increase the performance of radiative cooling in a completely energy-free manner. One successfully method employed the bi-directional emissivity of a cooling material. Its effectiveness is ascribed to the unique target situation, *i.e.*, an enclosed space at a very high temperature. There are three principles underpinning this. First, convection and conduction are generally the main heat transfer mechanism and dominates radiation. However, if the walls of an enclosed space are emissive, radiation can be maximized. Second, because the temperature increase of an enclosure space is mainly caused by the greenhouse effect, increasing IR-transmittance effectively prevents heat accumulation. Third, given that radiative heat dissipation is proportional to the fourth power of the temperature, sufficient radiative cooling power can be generated in the high-temperature enclosure. Thus, combined emissive and transmissive enclosure walls effectively allow the trapped heat to escape by enhancing the thermal radiation and preventing heat accumulation, respectively.

Radiative cooling material can be used as the walls or windows of the enclosed structure to enable space cooling (Fig. 4a). The materials used for enclosure walls reflect radiation in the solar range and emit IR radiation, which is similar to the requirements for building cooling. In terms of IR-emissivity, radiative cooling walls can be categorized as selective (emission in the ATW range and transmission at other IR wavelengths) or broadband emitters (emission at MIR-FIR). Previous studies focused on uni-directional radiative coolers that exhibit emissivity towards the outside and zero-emission on the inside of the enclosure, reflecting the inner radiation (Fig. 4b-i). Additional studies investigated radiative cooling with bi-directional emissivity, which can be divided into coolers having broadband absorption on the inside and selective emission on the outside (Fig. 4b-ii), and those exhibiting the same absorption or transmittance in both sides (Fig. 4b-iii). For instance, radiative cooling materials can be used as windows. Kim *et al.* proposed a transparent radiative cooler that transmits in the Vis. range, reflect NIR, and emits ATW radiation, thereby lowering the inside temperature during daytime (Fig. 4c).[81] As shown in Fig. 4d, the fabricated sample exhibited Vis.-transparency. A rooftop experiment was conducted with the absorbing chamber mimicking a car or a building that trapped sunlight transmitted through a transparent object. It was demonstrated that the transparent cooler could lower inside temperatures by up to 14.4 °C (Fig. 4e).

Heo *et al.* reported a Janus emitter that can absorb thermal input (above ambient temperatures, *e.g.*, 60 °C) in a broad spectral range, while the top side selectively emits heat to space without being disturbed by ambient radiation (Fig. 4f).[17] The cooling material consisted of, from top to bottom, a 4 μm polydimethylsiloxane (PDMS) layer, 100 nm silver layer, and a 500 μm-thick micro-patterned quartz layer coated with 10 μm PDMS (Fig. 4g). As shown in Fig. 4h, the proposed design has broadband emission on the bottom side to ensure broad absorption of inner thermal radiation, and selective emission on the top side that matched the ATW to minimize the disturbance from atmospheric radiation. Fig. 4i depicts an outdoor experimental setup molded in the shape of a car to demonstrate the space cooling with heating from solar radiation. The top of the setup is a perforated cover with the sample with a uni-directional cooler (composed of an Al plate coated with ~100 μm PDMS) and the Janus emitter. The setup with the Janus emitter achieved ~4 °C lower inner temperature compared to the uni-directional cooler (Fig. 4j). Similarly, Kim *et al.* fabricated a large-scale Janus emitter (20 cm) and confirmed that the thermal-managing properties were maintained regardless of chamber volumes.[82] Furthermore, it was demonstrated that the Janus emitter possessed thermostat properties by suppressing its cooling capability in lower temperature conditions (*i.e.*, night and winter). Liu *et al.* designed a biomimetic photonic multiform composite that exhibit 97.6% solar reflection and 95.5% IR heat emission (Fig. 4k).[83] A demonstration test was conducted considering potential scenarios for enclosure walls composed of porous thermoplastic polyurethane (TPU)-Al_2O_3 nanoparticles (NPs) composite slabs and commercial white acrylic plates (with broadband reflection in the Vis. range and emissivity of ~88% in the MIR range). As shown by thermal images in the Fig. 4l, the sample was maintained at a temperature 10 °C lower than that of acrylic plates (25 °C). Films consisted of randomly embedded alumina NPs in a porous matrix of TPU (Fig. 4m).

Research into greenhouse cooling has also been performed. The greenhouse is a building designed for cultivation sheltered from excessive cold or warm weather conditions and predators, allowing year-round production.[84] Methods for cooling a greenhouse during warm weather include providing cool air (*e.g.*, ventilators/vents), evaporated water, mechanical air conditioning, and reducing the intensity of incident light.[85] Fundamental optics are another simple solution; when a material is emissive, the majority of the internally generated photons are trapped inside the material.[86] In other words, the greenhouse can lower its inside temperature by the judicious choice of the material composing its wall. Cho *et al.* studied emissivity-dependent radiative heating phenomena.[87] They fabricated greenhouses covered with low- (0.34) and high-emissivity (0.86) polyethylene (PE) films and monitored the temperature on the inside of the greenhouses. Fig. 4n shows optical and thermal camera images of greenhouses covered with each film. The daytime temperature of the high-ε greenhouse was higher (maximally ~8 °C) than that of the low-ε greenhouse. In addition, the low-ε greenhouse cooled more during the nighttime than the high-ε greenhouse because of its higher transmittance of 5–8 and 13–17 μm wavelength radiation.

3.2 Personal thermal management: fabrics and wearable devices

3.2.1 Radiative cooling textiles. Radiative cooling fabrics/textiles for personal thermal management are discussed in this section. In the heat balance of the human body, convection/conduction heat transfer contributes ~40 W m^{-2} while radiative heat transfer accounts for ~25 W m^{-2}.[88] Although traditional textiles are good thermal emitters, their IR opacity inevitably functions as a radiation shield, hindering radiation from the skin. Therefore, IR-transparent textiles should be manufactured

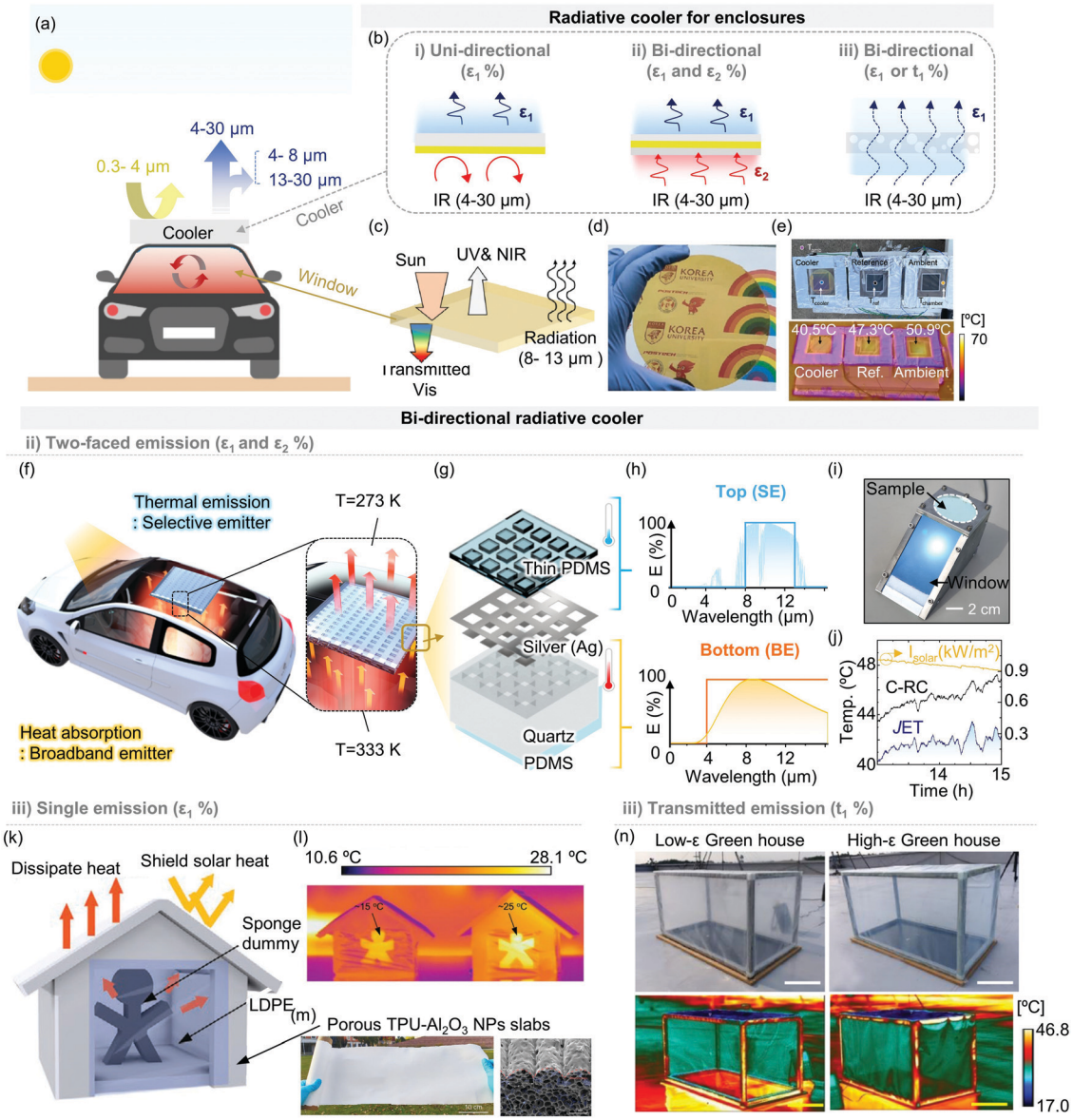

Fig. 4 Radiative cooling for enclosures. (a) Schematic illustration of a radiative cooler applied to an automobile under direct sunlight, where heat is trapped by the greenhouse effect. (b) Characteristics of suggested radiation properties in automobiles from recent studies. (c–e) Vis.-transparent radiative cooler applicable for car windows. Reproduced with permission.[81] Copyright © 2021. John Wiley & Sons, Inc. (c) Schematic of an ideal transparent radiative cooler that transmits Vis., reflects UV and NIR, and emits thermal energy *via* blackbody radiation in the ATW range. (d) Photograph of the cooler, confirming its transparency. (e) Photographs and thermal camera images of the rooftop measurement setup. (f–j) A Janus bi-directional emitter applied to a space cooling experiment. Reproduced with permission.[17] Copyright © 2020. AAAS (f) Schematic illustration of a radiative cooler under direct sunlight. (g) Magnified structural view of the cooler. (h) Desired radiation characteristics in automobiles. Emission spectra of the cooler with broadband emission (BE) on the bottom and selective emission (SE) on the top. (i) Rooftop measurement setup with heating by solar radiation molded in the shape of a car. (j) Temperature measurements of the radiative object. (k–m) A biomimetic multiform radiative cooler with transitive emissivity properties applied to a space cooling experiment. Reproduced with permission.[83] Copyright © 2020. John Wiley & Sons, Inc. (k) Temperature test simulating the potential scenario for cabins composed of a porous radiative cooler. (l) Temperature of the human-shaped sponge recorded by a thermal camera. (m) Photographs and scanning electron microscopy (SEM, oblique view) images of a large uniform film of a porous radiative cooler. Reproduced with permission. Copyright 2021. (n) Application of thermal radiation films with either low- or high-emissivity to a thermally insulating space where heat is trapped by the greenhouse effect. Optical (upper) and thermal (lower) camera images of the low- and high-emissivity greenhouses. Reproduced with permission.[87] Copyright © 2020. Elsevier B.V.

for achieving thermal comfort. Fig. 5a shows a scheme of radiative cooling textiles for personal thermal management. To achieve cooling, the textile should strongly reflect the solar spectrum and permit the transmission of thermal radiation from the skin. PE is considered as a key material for such textiles, because it exhibits transparency in the ranges from visible over the thermal wavelength region. Although IR transparency is inherent to PE, the solar spectrum should be reflected.

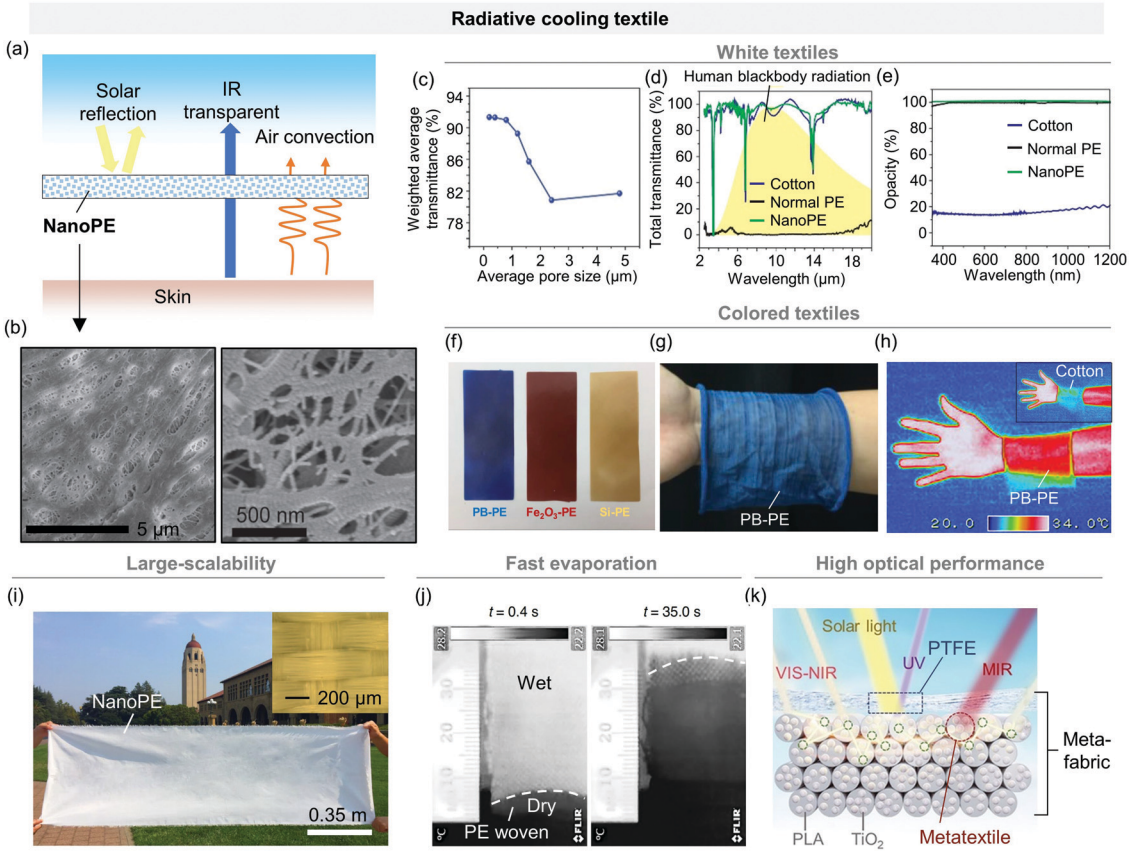

Fig. 5 Radiative thermal managing textiles for comfort. (a) Schematic illustration of the operating principles of cooling textiles. (b) SEM images for the cooling and heating mode of textiles. Reproduced with permission.[11] Copyright © 2016. AAAS. (c) Weighted average transmittance of thermal wavelength as a function of pore size. Reproduced with permission.[11] Copyright © 2016. AAAS. (d) Transmittance spectrum of cotton, normal PE, and nanoPE. Reproduced with permission.[11] Copyright © 2016. AAAS. (e) Visible opacity of cotton, normal PE, and nanoPE. Reproduced with permission.[11] Copyright © 2016. AAAS. (f) Photograph of the pigment nanoparticle-mixed PE composite films. Reproduced with permission.[96] Copyright © 2019. Cell Press. (g) Photograph of knitted textiles of PB-PE. Reproduced with permission.[96] Copyright © 2019. Cell Press. (h) Infrared images of human skin covered with PB-PE textiles. The inset shows the infrared image of human skin covered with cotton. Reproduced with permission.[96] Copyright © 2019. Cell Press. (i) Photograph of a large woven nanoPE fabric. Reproduced with permission.[105] Copyright © 2018. Nature Springer. (j) Infrared images of a water-immersed woven PE fabric sample showing advancement of the transition line between the wet and dry regions at different time points. Reproduced with permission.[106] Copyright © 2021. Nature Springer. (k) Schematic of a hierarchical metafabric for daytime radiative cooling. The blue, green, and red annotations highlight the three-level hierarchical structure corresponding to UV, VIS-NIR, and MIR bands, respectively. Reproduced with permission.[107] Copyright © 2021. AAAS.

To address this, Hsu *et al.* pioneered the nanoporous PE (nanoPE) textiles (Fig. 5b).[11] The nanopores induce strong Mie scattering in the visible range, which is the dominant range in the solar spectrum, and abundant pores in nanoPE remarkably increase solar reflectivity. The optimum-sized nanopores show high transparency in the thermal wavelength region because the nanopores function as sub-wavelength structures within the thermal wavelength region (Fig. 5c). The nanoPE textiles exhibit a high solar opacity, whereas it maintains a high transmittance in the LWIR region (Fig. 5d and e). In addition to cooling behavior, nanoPE offers excellent mechanical flexibility and softness.[11] Instead of nano-scaled air voids, ZnO NPs, an IR-transparent material, could be used to attain both high solar reflectivity and IR-transparency.[89] Furthermore, nanomesh textiles based on polyvinylidene fluoride (PVDF) fibers have been proposed using electrospinning for radiative cooling textiles.[90] However, the PVDF-based textiles exhibit IR-opacity and are thus useful to cool an object with low thermal emissivity. Other approaches have been reported to implement high solar-reflective and IR-emissivity textiles using 3d printable high-thermal conductive fibers,[91] electrospining,[92] wet spinning,[93] and nanoprocessed silk.[94] Moreover, biodegradable radiative cooling fibers were recently proposed to prevent ice from melting under sunlight.[95]

These radiative cooling textiles have a white surface color for maximizing solar reflectance. However, there is a need for colored textiles for aesthetic reasons. Cai *et al.* studied colored cooling textiles by doping inorganic NPs (*i.e.*, Prussian blue (PB), FE_2O_3, and Si) in PE fabrics (Fig. 5f).[96] Because NPs barely emit LWIR radiation, they can serve as color-pigment without IR absorption. Optical and thermal images of the PB-PE textile are shown in Fig. 5g and h, respectively. As a control, cotton textile with low IR-transparency shows a low temperature (*i.e.*, thermal energy from the skin is trapped; Fig. 5h, inset). In contrast, a high skin temperature is

evident through the PB-PE textile (Fig. 5h). Coloration is inevitably accompanied by solar absorption. As a result, colored radiative heating textiles have been reported.[97–101] In addition to solar absorption, IR opacity was introduced into the textiles using various photonic configurations to hinder radiative heat loss from the body. Examples include Ge/Au structures,[97,102] polymer/oxide composite fiber,[98,103] and metal–polymer composite textiles.[99,100,104]

Fig. 5i shows a large-scale woven nanoPE fabric and the magnified image in Fig. 5i shows the detailed pattern of woven nanoPE.[105] This woven pattern enhances the spectral features (*i.e.*, transmittance in the LWIR region) and mechanical properties (*i.e.*, wearability and durability) compared to those of conventional film structures (*i.e.*, without woven pattern). This woven nanoPE fabric lowers skin temperature by 2.3 °C, corresponding to a greater than 20% saving on indoor cooling energy consumption. Moreover, PE fabrics can be fabricated into multifilament yarns for excellent strain resistance, efficient moisture-wicking, and fast-drying of textiles (Fig. 5j).[106] In water-wicking tests, woven PE fabric excelled with the transition line receding a distance of ~10 cm in 10 min compared to those of commercial natural (cotton ~9.5 cm, linen ~8 cm) and synthetic (polyester ~7 cm) textiles. This excellent moisture transportation feature results from the combination of fiber surface properties, the average diameter of the fibers, and yarn composition. This leads to passive evaporative cooling as well as passive radiative cooling, which is helpful for heating, ventilation, and air-conditioning (HVAC) energy savings as well as personal thermal comfort. In addition to single-material PE textiles, highly-emissive so-called metafabrics that combine different materials, such as polylactic acid (PLA), TiO_2 NPs, and PTFE, have also been reported (Fig. 5k).[107] The PTFE nanofibers with TiO_2 NPs are responsible for reflecting sunlight, including UV, Vis., and NIR radiation. The PLA microfibers strongly emit thermal radiation in the LWIR range. Possessing tailored optical hierarchical structures, this metafabric can cool skin temperature by ~4.8 °C more than cotton fabric.

The materials, photonics, and mechanical efforts employed to realize more efficient radiative cooling textiles provide guidance to the commercialization of radiative cooling textiles. However, heating and cooling needs vary depending on ambient temperatures. Therefore, mode-switchable smart textiles are more practical. Recent progress on the development of smart textiles was recently brought to fruition, as discussed in Section 3.5.

3.2.2 Wearable devices. Advances in flexible/stretchable electronics have enabled their implementation in wearable form. Such body-worn electronic systems have been widely used to monitor various biological signals in real-time (*e.g.*, sweat,[108] humidity,[109,110] UV dosimeter,[110] oximeter,[111] electrocardiac,[112–114] strain,[114,115] tactile,[116] and stress sensors[117]). To achieve these multi-functionalities, diverse active elements are used, including transistors, operational amplifiers, diodes, and field-programmable gate arrays, and they can generate undesirable heat. Among them, photoplethysmography (PPG) sensors (*e.g.*, pulse and tissue oximeters) include light sources, such as light-emitting diodes (LEDs) and photodiodes. The light source can unintentionally act as a heating source as well.[118–120] In addition to such internal heat sources, an external heat source exists in the outdoors, that is, sunlight. Because ambient light is a source of noise for PPG sensors, black encapsulations often cover these sensors to shield them (Fig. 6a, left). In this situation, the black layer strongly absorbs sunlight and the resultant increased temperature can damage skin[119,121–123] or degrade the device performance.[124–126] Radiative cooler-integrated wearable devices were recently reported to address this issue (Fig. 6a, right).[127,128]

To integrate a radiative cooler with wearable devices, the radiative cooler must be flexible/stretchable. In addition, for wireless communications, a metal layer should not be included in the radiative cooler. Xu *et al.* reported a suitable radiative cooler that satisfies these requirements (Fig. 6b).[127] The proposed radiative cooler has multiple functionalities, such as high stretchability, breathability, softness, and waterproof features. The multifunctional radiative cooler was fabricated using a phase-inversion process of polystyrene-*block*-poly(ethylene-*ran*-butylene)-*block*-polystyrene (SEBS), isopropyl alcohol (non-solvent), and chloroform (solvent), which is a simple, inexpensive, and scalable method. The inset of Fig. 6b displays the porous structure of the radiative cooler. The abundant micropores offer high solar reflectivity while maintaining low reflectivity in the LWIR region (Fig. 6c). Owing to the scale difference between micropores and wavelengths, sunlight is strongly reflected. In contrast, these micropore structures function as a sub-wavelength structure within the LWIR region.

As a practical application of radiative coolers for wearable devices, Kang *et al.* demonstrated a thermally stable patch-type tissue oximeter with radiative coolers (Fig. 6d).[128] The radiative coolers hierarchically consisted of SEBS and poly(methylmethacrylate) (PMMA) with nano-/micro-voids polymers (NMVPs). The hierarchical layout of the NMVP increases solar reflection and LWIR emissivity owing to multiple Mie scattering and the anti-reflection effect, respectively. Fig. 6e shows the appearances and temperatures of black elastomer (BE), white elastomer (WE), and NMVP on skin. After 8 min exposure to sunlight, the temperatures of BE and WE raised to ~40 and ~35 °C, respectively, while NMVP maintains a near-indoor skin. Fig. 6f compares the temperatures and muscle oxygen saturation (StO_2) values measured by the BE- and NMVP-integrated patch-type tissue oximeters. The exposure of devices to sunlight during 4 min without any exercising (*i.e.*, the subject is idle) increases the temperature of the BE-integrated device to 38.1 °C. As a result, the measured StO_2 value shows an erroneously low value, ~68%. However, the NMVP-integrated device maintains the temperature as 33.1 °C and an accurate idle StO_2 value is measured, ~80%. While other studies attempted to deal with the self-heating issue of the device for example using a PCM[129] and thin-metallic heat sink,[130] this work is the first demonstration to address this issue in an outdoor environment and shows the potential solution for cooling wearable devices. Using convection and conduction to cool the wearables may have limitations because progress in wearable devices has focused on developing small- and ultra-

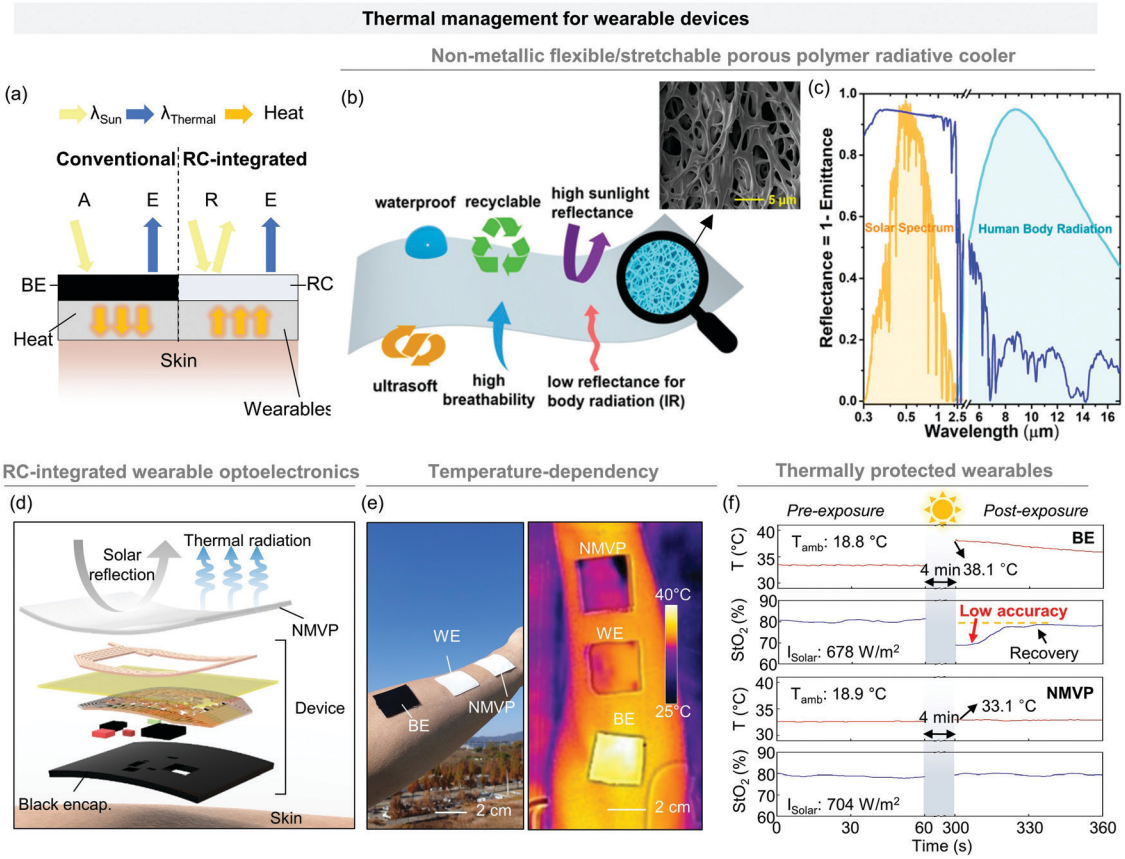

Fig. 6 Thermal management of radiative coolers for wearable devices. (a) Schematic illustration of operating principles of conventional and radiative cooler-integrated wearable devices. (b) Schematic illustration of the non-metallic flexible/stretchable radiative cooler based on a porous polymer. The inset shows a SEM image of the radiative cooler. Reproduced with permission.[127] Copyright © 2020. National Academy of Sciences. (c) Reflectance spectrum of the porous SEBS substrate between 0.3 and 17 μm. Reproduced with permission.[127] Copyright © 2020. National Academy of Sciences. (d) Schematic illustration of a radiative cooler-integrated wearable optoelectronic device. Reproduced with permission.[128] Copyright © 2021. Wiley-VCH. (e) Photograph (left) and thermal image (right) of samples such as black elastomer (BE), white elastomer (WE), and nano/micro-voids polymer (NMVP). Reproduced with permission.[128] Copyright © 2021. Wiley-VCH. (f) Comparison of measurements pre-exposure and post-exposure with a BE-integrated device and NMVP-integrated device attached to the forearm. Blueish regions represent the period (4 min) of direct sunlight exposure. Reproduced with permission.[128] Copyright © 2021. Wiley-VCH.

thin forms. Therefore, thermal management is becoming increasingly essential in advanced wearable devices with high device integration and operating speeds, and the importance of heat transfer through radiation may increase.

3.3 Energy harvesting: solar cells and thermoelectric generators

The coldness of the universe can enable radiative cooling, but it can also provide a new class of energy harvesting.[131–134] The radiative heat exchange between a radiative cooler and the universe can generate electrical power, which results from a negative illumination effect.[132] This effect is in contrast with the positive illumination for energy harvesting, which is the operating mode of solar cells. Several studies have theoretically demonstrated the thermodynamic limits of harvesting power from thermal radiation from the ambient environment to the universe. In particular, a system with a number of circulators showed a theoretical power generation of over $\sim$140 W m^{-2}.[133] Ono *et al.* experimentally demonstrated electrical power generation from coldness harvesting using the negative illumination effect.[134] However, radiative coolers can maximize the efficiency of energy harvesting when the cooler is applied to other energy harvesting devices *via* the synergetic effect. The following sections discuss radiative cooler-integrated energy harvesting devices.

3.3.1 Solar cells. Solar cells most benefit from the introduction of radiative coolers. Solar cells convert solar energy into electricity through the PV effect. For silicon-based single-junction solar cells, the maximum efficiency is approximately 33.7% based on the analysis by Shockley and Queisser.[135] Therefore, only a fraction of the absorbed solar energy is converted into electricity with the remainder eventually becoming heat, increasing the operating temperature. It is well known that the efficiency and lifetime of solar cells are degraded by high temperature. The relative efficiency of crystalline silicon solar cells is estimated to drop 0.4–0.5% for every 1 °C temperature increase.[136] Thus, maintaining a low temperature is a major concern to ensure the optimum energy output of solar cells.

Earlier works on cooling technologies for solar cells include heat pipe,[137] airflow,[138,139] water flow,[140] PCM,[141] passive heat sink,[142] and micro-channel.[143] However, radiative cooling of solar cells is relatively straightforward because it is cheap, passive, and lightweight. Furthermore, it has been shown that radiative cooling is more resilient to high temperatures than other cooling methods (*i.e.*, relying on convection and conduction) because the radiative cooling power scales much faster (proportional to the fourth power of the temperature difference) as temperature increases. From a materials viewpoint, bare silicon has low IR-emissivity, *i.e.*, silicon solar cells do not have a radiative self-cooling feature. Since the silicon solar cell is still the mainstream product in the current PV industry, integrated solar cell-radiative cooler units are practical. Thus, the solar cell can potentially work stably under strong sunlight in conjunction with radiative cooling.

A common approach for radiative atmosphere cooling of solar cells is to place a material on top of the solar cell which is designed to have two main radiative properties (Fig. 7a). First, it has high transmittance in the solar spectrum (0.3–4 μm) to enable the solar cell to generate maximum electricity. Second, the cooling material should be highly emissive over the IR spectrum (4–30 μm) to maximize cooling power. Note that a blackbody emission at a longer wavelength is more suitable for dissipating low-grade heat from a solar cell, because it has an elevated working temperature. Based on previous studies, there are two structural groups proposed for radiative solar cell cooling, *i.e.*, multilayer- and metamaterial-based radiators, as illustrated in Fig. 7b and c.

Multilayer-based radiators are one-dimensional photonic structures that consist of alternating dielectric layers of high and low refractive indices. These structures reflect sub-bandgap solar radiation (*i.e.*, in the MIR range) to reduce parasitic heat generation and also have high emissivity in the IR range.[144] Li *et al.* devised a multilayer dielectric cooler on top of a crystalline silicon solar panel (Fig. 7b).[20] They encapsulated a typical solar cell with two 0.46 mm-thick ethylene-vinyl acetate (EVA) joint interlayers and a 3.2 mm-thick glass front cover. The photonic cooler was designed to have maximal reflection in the NIR range and strong thermal emission in the MIR-FIR range by alternating Al_2O_3/SiN/TiO_2/SiN with a single top layer of SiO_2.

Metamaterial structures have also been explored as a radiative cooler design for solar cells. Because they have a higher degree of freedom (*i.e.*, width, period, depth, *etc.*) than one-dimensional multilayer structures, metamaterial radiators have broader boundaries for tailored optical characteristics. Zhu *et al.* experimentally demonstrated that a SiO_2 metamaterial achieved strong heat radiation of silicon solar cells.[33] The structure also assures Vis-transparency. The SiO_2 photonic crystal was fabricated to have a square lattice with a periodicity of 6 μm with an etching depth of 10 μm, as shown in the scanning electron microscopy (SEM) image in Fig. 7c.

It has been established that strong resonance takes place between electromagnetic radiation and materials possessing structures on a scale corresponding to the wavelength of the incident light.[145] Therefore, structures with multiple dimensions offer more possibilities to realize an optimized optical performance. Perrakis *et al.* reported a nano- and micro-scaled patterned cooler that improved radiative cooling and the efficiency of the solar cell.[146] The microstructure was designed to enhance LWIR heat emission, whereas the nanostructures acted as an anti-reflective coating in the solar range. The result showed a ~3.1% increase of silicon solar-cell efficiency and ~5.8 °C of cooling, on the bases of their simulation model. Several recent studies demonstrated passive cooling coupled with solar radiation management. Heo *et al.* reported a two-dimensional SiO_2 metasurface radiative cooler that served both cooling and light trapping (Fig. 7d).[147] The power distribution of radiative cooler-integrated solar cell is illustrated in Fig. 7e, where the cooler was designed to have an emissivity that encompasses the entire LWIR–FIR range. The experimental results were a ~1.3% increase in efficiency and ~6 °C cooling of the InGaP/GaAs/Ge multi-junction solar cell. The optical image supported the light trapping effect through diffraction at the visible spectrum (Fig. 7f). The thermal image in Fig. 7g implied that the sample also has a high thermal emission. They also studied the parasitic heating from the absorption of sub-bandgap photons and theoretically demonstrated that a multi-junction solar cell is immune to heating by sub-bandgap photons. Lu *et al.* suggested versatile ultra-broadband textures *via* a modified sol–gel imprinting method that interacted with Vis.-FIR radiation.[148] As shown in Fig. 7h, the geometric diffraction in the solar spectrum led to light trapping, which resulted in 5.12% and 3.13% relative enhancements of the short-circuit current and solar-cell efficiency, respectively. Furthermore, the pyramidal textures supplied gradient-index sub-wavelength structures to suppress IR-reflection. As a result, near-unity emissivity over 96% was obtained in the MIR–FIR ranges. The solar-managing design was also targeted to obtain high transmittance in the Vis.-NIR range. Lin *et al.* reported flexible photonic architectures (FPA) on PDMS by mimicking the hierarchically photonic architectures of silver ant hairs.[149] The FPA-PDMS device not only has a large emittance in the MIR-FIR range, but also a high transmittance in the Vis.-NIR range in comparison with those of glass, which could potentially improve the entry of sunlight and the dissipation of heat in solar cells.

Apart from single solar cell cooling devices, cooling of system-units, such as the extraterrestrial PV system,[150] thermal PV system,[151] and concentrated photovoltaic (CPV) system,[151] has also been demonstrated. Wang *et al.* studied the light-weight radiative cooling performance of CPV.[31] The experimental setup is illustrated schematically in Fig. 7i. Electrodes and thermocouples were mounted to the solar cells in chambers 1 and 2 to measure their open-circuit voltage (Fig. 7j). The photograph in Fig. 7k shows the light beam focused on the center of the solar cell. Multiple outdoor experiments revealed that radiative cooling could contribute approximately 25% to 62% of the overall cooling power of a CPV system. Zhou *et al.* further improved the concept for CPV cooling by studying a low-bandgap PV, which is closely related to CPV and TPV

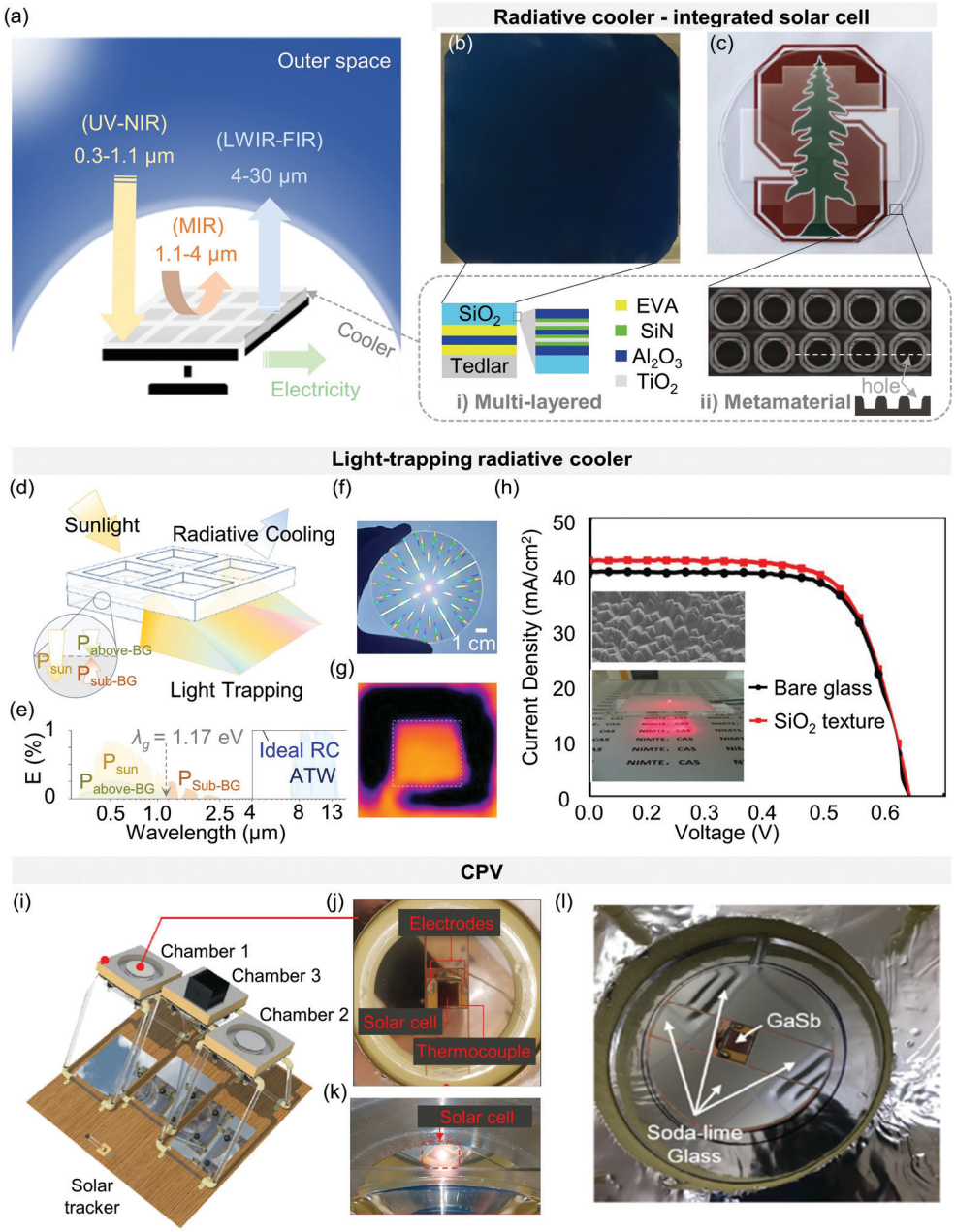

Fig. 7 Radiative cooler-integrated solar cells. (a) Schematic illustration of a passive radiative cooling system integrated with a solar cell. The ideal radiative cooler for a solar cell should absorb UV-Vis., reflect NIR, and emit MIR radiation. (b and c) Two representative structures for cooling the solar cell: (b) multi-layered structure on silicon solar cell (reproduced with permission.[20] Copyright © 2017. American Chemical Society), and (c) metamaterial (reproduced with permission.[33] Copyright © 2015. National Academy of Sciences). (d–g) A radiative cooler that cools as well as improves the efficiency of the solar cell. Reproduced with permission.[147] Copyright © 2021. John Wiley & Sons, Inc. (d) Illustration of a radiative cooler which simultaneously radiates heat and traps light. (e) Power distribution in a solar cell integrated with a radiative cooler. (f) Photograph and (g) thermal images of the cooler. (h) Transmission haze of the control and imprinted texture glass. The inset is the SEM image and photograph of texture glass shined on by a laser pointer. Reproduced with permission.[148] Copyright © 2017. John Wiley & Sons, Inc. (i–k) Radiative cooler applied to a concentrated photovoltaic (CPV) solar cell. (i) Schematic illustration of tracing solar rays with chambers. (j) Photograph of the electrodes and thermocouples connected to the solar cell. (k) Photograph showing the focused beam falling on the center of the solar cell. (Reproduced with permission.[31] Copyright © 2020. Cell Press). (l) Photograph of the structure in a cooling assembly consisting of a PV diode (GaSb) and the soda-lime glass radiative cooler. Reproduced with permission.[152] Copyright © 2019. Optica Publishing Group.

applications.[152] They demonstrated enhanced radiative cooling on low-bandgap GaSb PV cells under concentrated sunlight. Radiative cooling reduced operating temperatures by 10 °C in the experimental setup shown in Fig. 7l, which corresponds to a 5.7% relative increase in the open-circuit voltage and an estimated 40% increase in lifetime at 13 suns.

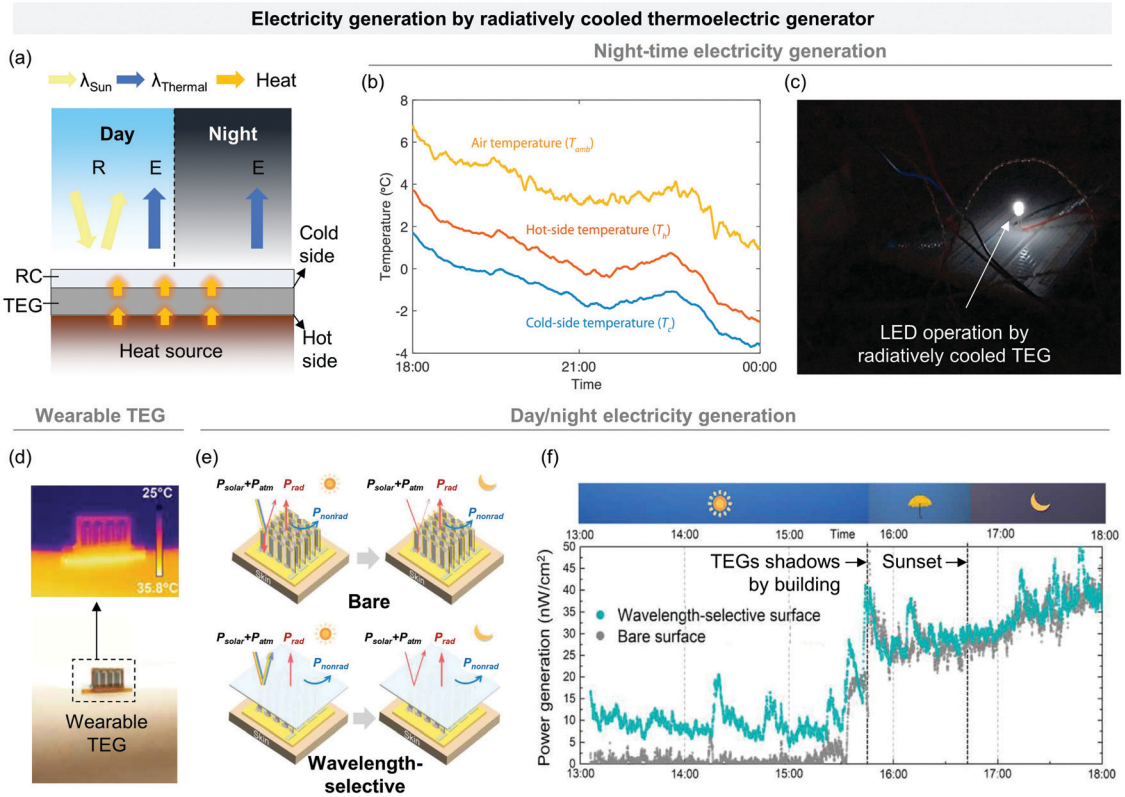

Fig. 8 Electricity generation by a radiatively cooled thermoelectric generator. (a) Schematic illustration of the operating principles of radiatively cooled thermoelectric generators (TEGs). (b) Temperature values of the hot and cold sides of the TEG along with the ambient temperature. Reproduced with permission.[21] Copyright © 2019. Cell Press. (c) Picture of the LED operating at night, powered by the radiatively cooled TEG. Reproduced with permission.[21] Copyright © 2019. Cell Press. (d) Optical (bottom) and thermal (top) images of a wearable TEG on an arm. Reproduced with permission.[159] Copyright © 2021. AAAS. (e) Schematic illustration of heat-transfer processes of TEGs with bare and wavelength-selective surfaces during the day- and nighttime. P_{Solar} and P_{atm} are the solar and atmospheric radiation power incident on the surface, respectively, P_{rad} is the thermal radiation power from the surface, and P_{nonrad} is the non-radiative heat transfer. Reproduced with permission.[159] Copyright © 2021. AAAS. (f) Power generation of the TEGs with bare and wavelength-selective surfaces at the cold side. Reproduced with permission.[159] Copyright © 2021. AAAS.

3.3.2 Thermoelectric generators. With rapidly increasing climate change, the world is eager to secure eco-friendly and reusable energy sources to reduce carbon emissions. PV technology is already mature and verified, however it cannot be used at night, so there is an imbalance in power generation. Radiative cooling can be a promising solution to address this issue. A radiatively cooled surface can be exploited to generate electricity by combining it with a thermoelectric generator (TEG). By integrating a daytime radiative cooler with TEGs, a prominent temperature difference can be achieved in day- and nighttime (Fig. 8a).[21,153–157]

Raman *et al.* first demonstrated electricity generation in nighttime using a low-cost TEG with a simple thermal emitter. The thermal emitter was composed of a 200 mm aluminum disk, covered with a black paint with an emissivity of ~0.95, attached to a commercial TEG.[21] Fig. 8b shows the temperature of hot and cold sides of the device that were ~2 °C and 4–5 °C cooler than ambient air, respectively. Although the hot side had no radiative cooling effect and only experienced convective heat transfer with ambient air, a conductive heat flow from it to the cold side reduced the temperature difference between the sides. However, notwithstanding the reduced temperature difference, the power generated was 25 mW m^{-2}, which was enough to power a LED (Fig. 8c). In another study, the radiative cooler/TEG could generate electricity not only during nighttime, but also the daytime, using a simple glass/Al structure.[158]

There is ongoing effort to develop wearable forms of TEGs to power wearable electronics and generate electricity from body heat.[157,159–161] Fig. 8d displays a wearable TEG that uses body heat to generate electricity.[159] The thermal image exhibits a notable temperature difference in wearable TEG. This TEG has stretchability, self-healing ability, recyclability, and Lego-like reconfigurability that can be merged with separated TEG devices in series or parallel form. The authors demonstrated outdoor usability by integrating the TEG with a wavelength-selective metamaterial film (*i.e.*, a radiative cooler; Fig. 8e). The bare TEG surface has a strong solar absorption (>0.87) in the 0.3–2.5 μm range. In contrast, the wavelength-selective film minimizes solar absorption. Owing to these spectral features, the TEG integrated with the wavelength-selective surface enables all-day electricity generation (Fig. 8f).

From the findings discussed earlier, greater power generation can be realized when the radiative cooling is applied to TEGs that uses body heat. In addition, this functionality may be

implemented in clothes comprising radiative cooling/heating textiles. Moreover, in wearables, this approach can be used to control the thermal management of the device while simultaneously supplying electricity to operate the device.

3.4 Dew harvesting

Humid air naturally condenses if the temperature of a surface is lower than the dew point of air (Fig. 9a). Because the collection of dew is cost-effective and minimally affected by geographical constraints compared with other atmospheric water harvesting technologies (*e.g.*, artificial rain and fog water collection), it is considered the most practical means of water harvesting—particularly in arid and semi-arid regions.[162] Some plants and animals, such as beetles, lizards, *Stipagrostis sabulicola*, and *Opuntia microdasys*, show great tolerance to live in hot and arid regions by direct water harvesting from the air.[163] Although dew is a frequent phenomenon, making it an abundant water resource accessible everywhere on the earth, it has long been overlooked due to its low yield.[164] In 1957, Monteith thoroughly outlined the energy and heat balance mechanisms of dew formation.[165] Since then, continued efforts have now enabled efficient dew collection.[162,166] Current dew collectors are classified as passive and active condensers. Among the remaining challenges, high yield is a key issue for passive dew harvesting.[163] Dew collection can be improved by lowering the condensing temperature and optimizing weather conditions. Fig. 9b summarizes weather and material parameters that influence passive dew collections.[167] Dew forms more favorable from clear skies, radiative surfaces with high IR ($\lambda \approx$ 8–13 μm)-emission, and low wind speeds (in the range of 0.15–0.7 m s^{-1}).

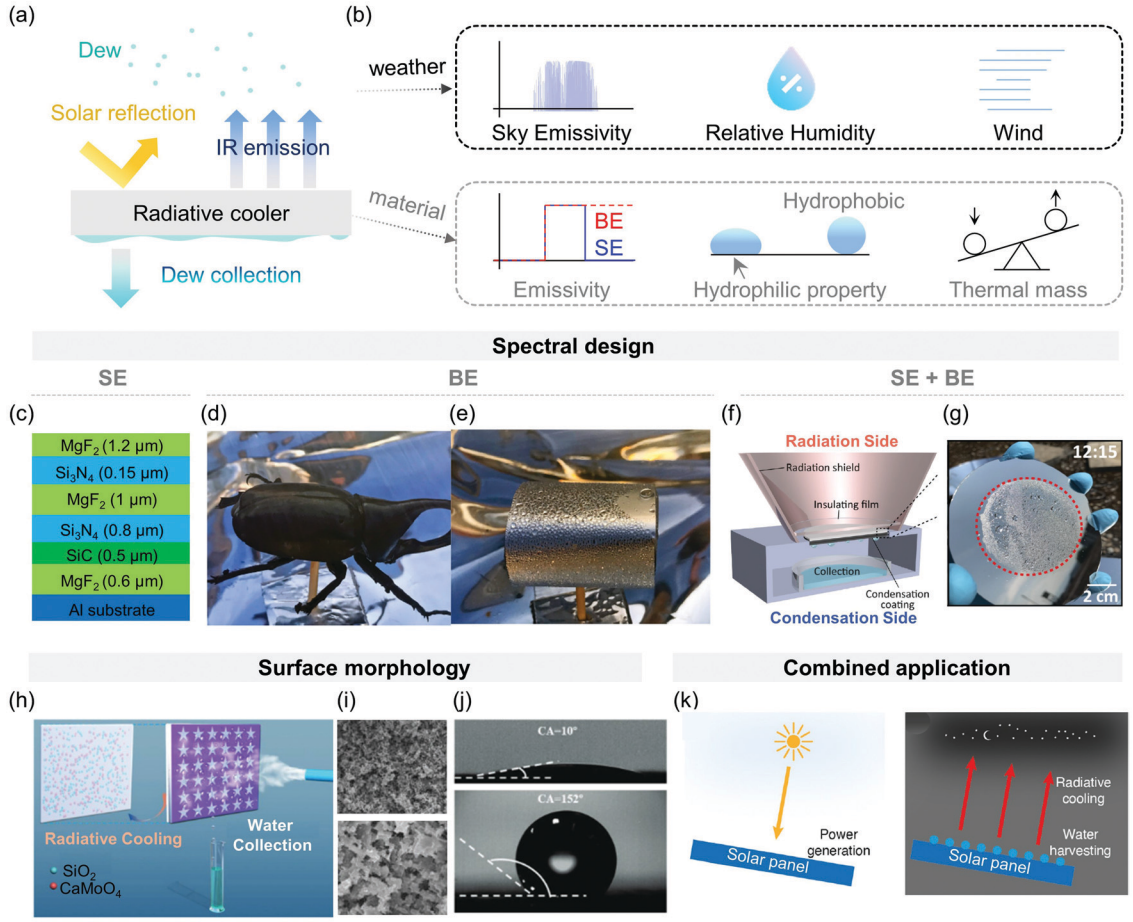

Fig. 9 Radiative cooler for dew harvesting. (a) Schematic of net radiation flux enabling daytime dew formation. (b) Factors that affect dew harvesting. (c) Cross-sectional view of a proposed design of a selective emitter. Reproduced with permission.[170] Copyright © 2020. Informa UK Limited (d) Photographs of a black beetle. Reproduced with permission.[14] Copyright © 2015. National Academy of Sciences. (e) Photographs of a daytime-condensing device that reflects most sunlight. Reproduced with permission.[14] Copyright © 2021. (f) Working principle of separated radiation and condensation sides. The radiation shield improves the dew harvesting potential of the system by accounting for the surrounding radiative environment. Reproduced with permission.[171] Copyright © 2021. AAAS. (g) Qualitative photograph of a dew-harvesting experiment under direct solar radiation. Reproduced with permission.[171] Copyright © 2021. AAAS. (h) Schematic of water harvesting with a radiative cooling coating on the back of the water collection surface. Reproduced with permission.[172] Copyright © 2020. Wiley-VCH. (i) SEM images of the electrochemically etched Al sheet for 11 min. Reproduced with permission.[172] Copyright © 2020. Wiley-VCH. (j) Contact angle of the surfaces of the star-shaped patterns (top) and the rest area modified by hexadecyl trimethoxysilane (bottom). Reproduced with permission.[172] Copyright © 2020. Wiley-VCH. (k) Schematic illustration of a solar panel for daytime power generation (left) and nighttime water harvesting (right). Reproduced with permission.[173] Copyright © 2020. American Chemical Society.

Because condensers with a higher mass have higher thermal inertia, low-mass materials are more advantageous for dew harvesting.[167] In addition, hydrophilic surfaces are needed to lower the energy barrier for nucleation.[164] Another property that affects dew harvesting is relative humidity (RH). Some researchers have found that water mostly condensed when the RH is between 74% and 92%.[168] However, the heat emission of radiative surfaces is hindered when a lot of water vapor is present in the sky. Museli *et al.*[169] concluded that net radiation should be considered as well as the RH in dew yield.[167]

Dong *et al.* reported performance limits of dew-harvesting technology by carefully considering RH, spectral directional atmospheric transmittance, ambient temperature, and the convection coefficient.[170] They highlight that a selective emitter that has high emissivity only at the ATW, has more condensing potential for arid conditions than a blackbody emitter. In their calculations, a near-ideal selective emitter could achieve a dew-harvesting mass flux of 13 g $(m^2\ h)^{-1}$ even at $T_{ambient}$ = 20 °C with RH = 40%, whereas the broadband emitter could not operate. They proposed a six-layered cooler to achieve optimized dew harvesting properties by selective emission (Fig. 9c). Since the importance of cooling power has emerged due to latent heat, Zhou *et al.* highlighted the need for a broadband emitter that has more than double the cooling power when compared to selective emitters.[14] They demonstrated a condenser that exhibits absorption in the Vis. and NIR regions while maintaining most of its thermal radiation in the LWIR to FIR ranges (*i.e.*, a broadband emitter). Unlike a black beetle that absorbed most of the sunlight (Fig. 9d), the devised condenser can achieve a temperature lower than ambient and can produce water for 24 h a day. As a result, they condensed ~8.5 mL day^{-1} of water for 800 W m^{-2} of peak solar intensity (Fig. 9e). Haechler *et al.* optimized a system that can achieve the advantages of both selective and broadband emitter designs.[171] They synergistically combined radiative shielding and cooling to achieve sub-ambient cooling while sustaining a high cooling power (for latent heat uptake). An engineered truncated cone-shaped structure was placed around the radiative cooler that acted as a radiation shield by directing thermal radiation from the selective emitter towards the normal incidence and simultaneously strongly truncates detrimental atmospheric radiation gains (Fig. 9f). For solar irradiance of 200 W m^{-2} and at a mean RH of 96%, the system achieved a dew-mass flux of 52 g $m^{-2}\ h^{-1}$ (Fig. 9g).

A multifunctional efficient water collection device had been demonstrated by Chen *et al.*[172] The fabricated sample consisted of a wetting pattern on one side of an Al sheet for efficient water harvesting, and a P(VDF-HFP) coating with embedded SiO_2 and $CaMoO_4$ NPs on the other side for cooling (Fig. 9h). The patterns were electrochemically etched on the Al sheet, as shown in the SEM images of Fig. 9i. As a result, hydrophilic patterns were obtained Fig. 9(j). They investigated the effect of circle, triangle, and five-pointed star wetting patterns on the water collection performance and found that the five-pointed star pattern was the most efficient, achieving ~0.42 g $cm^{-2}\ h^{-1}$. Li *et al.* proposed practical dew harvesting applications by combining the concepts of daytime power generation and nighttime water harvesting.[173] Unlike typical solar panels that only work in the daytime (Fig. 9k, left), the proposed solar panel uses radiative cooling with high thermal emissivity for dew harvesting at night (Fig. 9k, right).

3.5 Radiative self-adaption

In addition to cooling, temperature-regulation should be considered to minimize the annual energy consumption. For example, in the United States, ~39% of the total energy is consumed for thermal regulations in buildings.[174] Among them, the residential housing energy accounts for ~51% of energy consumption for maintaining a comfortable indoor temperature, ~22 °C.[175] In this context, thermal management for buildings requires not only cooling, but also heating depending on weather conditions. However, the previously discussed radiative cooling methods have fundamental limitation for addressing this. Therefore, self-adaptive radiative cooling/heating technologies should be developed to tackle these challenges. This section discusses two representative examples: (1) temperature-adaptive radiative coatings/windows using PCMs and (2) dynamic tunable IR gating textiles using hydrophilic–hydrophobic side-by-side metafibers.

Although PCM-based radiative structures to achieve self-adaptive radiative thermostats have been regularly reported, these are restricted to theoretical studies.[176–178] In addition, the high operating temperatures of PCMs hindered the development of self-adaptive thermostats.[179,180] In fact, PCMs are commonly used in IR camouflage applications.[181] However, Tang *et al.* recently experimentally reported a temperature-adaptive radiative coating (TARC) for all-season household thermal regulation.[75] The TARC automatically switches the emissivity in the LWIR range from 0.9 to 0.2 as the temperature of the TARC decreases below the temperature of the metal-insulator transition (T_{MIT}; Fig. 10a). To tailor T_{MIT}, the composition of the PCM $W_xV_{1-x}O_2$ was set to x = 1.5%.[182] In addition to the composition, two-dimensional micro-arrays of thin $W_xV_{1-x}O_2$ blocks were embedded in BaF_2 layers to optimize the spectral features and maximize the emissivity difference between the insulator- (*i.e.*, heating mode) and metal-states (*i.e.*, cooling mode). Fig. 10b shows thermal images of the TARC at three different temperatures. Low- and high-emissive samples (*i.e.*, $\varepsilon \approx 0.1$ and 0.95, respectively) are shown for comparison at the same temperatures. The emissivity switching of the TARC above or below T_{MIT} is evident. A 24 hour outdoor measurement further demonstrated the emissivity switching of TARC (Fig. 10c). During the daytime, although the white roof coating shows better cooling performance than TARC under direct sunlight (*i.e.*, fully exposed), the TARC manages the temperature depending on the ambient temperature (*i.e.*, with direct solar radiation blocked). As a result, the TARC achieves lower temperature than ambient air from 14:00 to 16:00 and a temperature closer to ambient air from 16:00. Another approach based on PCMs is radiative cooling regulating thermochromic (RCRT) smart windows, which addresses one of the least energy efficient parts of a building.[74] The RCRT regulates indoor temperatures by modulating both NIR-transmittance and FIR-emissivity using VO_2. More specifically, in summer, the NIR and FIR radiation is blocked and strongly emitted by the RCRT due to

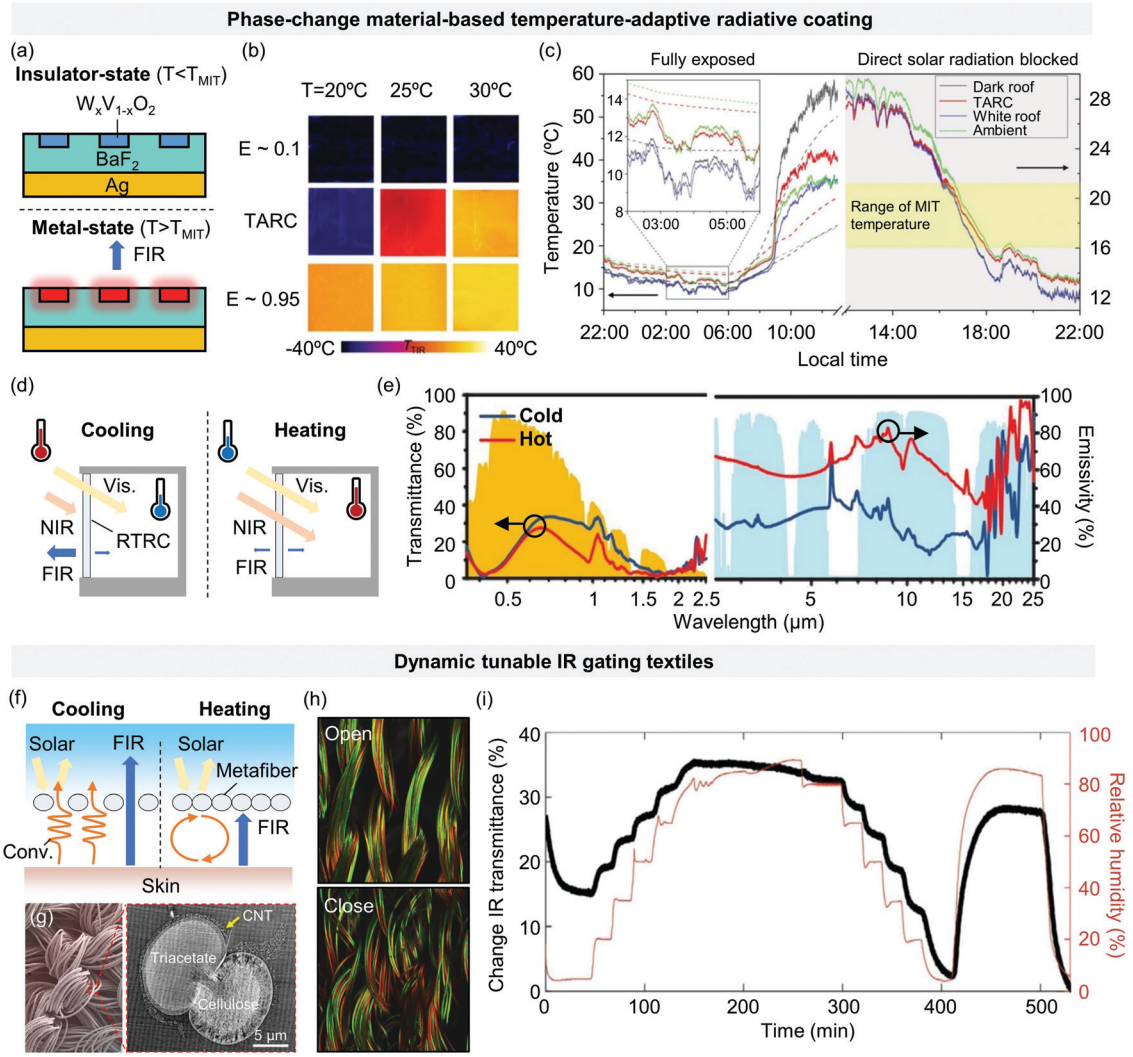

Fig. 10 Self-adaptive radiative coating, window, and textile. (a) Working mechanism of the TARC. When the temperature of TARC is above T_{MIT}, the FIR emission occurs. Reproduced with permission.[75] Copyright © 2021. AAAS. (b) Thermal images of TARC compared with those of two conventional materials with low or high thermal emissivity such as ~0.1 and 0.95. Reproduced with permission.[75] Copyright © 2021. AAAS. (c) Surface temperature of TARC, a commercial dark roof coating, and a commercial white roof coating in an open-space outdoor environment recorded over a day-night cycle. Measurements starting from 14:00 local time were performed with the direct solar radiation blocked. The temperatures observed after sunset show clear signs of the TARC shutting off thermal radiative cooling as its surface ambient temperature falls below T_{MIT}. Reproduced with permission.[75] Copyright © 2021. AAAS. (d) Working principle of the RCRT window in hot (left) and cold (right) weathers requiring cooling and heating, respectively. (e) Spectral of RTRC at 20 and 90 °C. Reproduced with permission.[74] Copyright © 2021. AAAS. (f) Working principle of self-adaptive textile. Metafibers become tight when the environment is hot or wet weathers and it works oppositely. (g) SEM image for the textile knitted by yarn composed of multiple metafibers. An enlarged TEM image shows the cross-sectional view of single-metafiber. Reproduced with permission.[188] Copyright © 2021. AAAS. (h) Confocal fluorescent microscopy images showing the knitted fabric in the closed state (*i.e.*, low humidity) and the open state (*i.e.*, high humidity). The hydrophilic cellulose component was dyed with an aqueous solution of rhodamine B (red), and the hydrophobic triacetate component was dyed using coumarin 6 (green). Reproduced with permission.[188] Copyright © 2021. AAAS. (i) Spectrum variation of IR gating textiles (black line) at different humidity profiles. The IR transmittance was averaged over 8 to 14 μm. Reproduced with permission.[188] Copyright © 2021. AAAS.

its low NIR-transmittance in and high FIR-emissivity (Fig. 10d, left). In contrast, the NIR and FIR are transmitted and barely emitted by RCRT in winter to trap heat inside (Fig. 10d, right). Such spectral tunability can be implemented by using differently emissive sides (Fig. 10e). The cold and hot states correspond to the temperatures of 20 and 90 °C, respectively.

For personal thermal management using textiles, mechanically-induced adaptive textiles have been reported as (i) dual-mode textiles with passive radiative heating/cooling capability,[183–186] and (ii) strain-based adaptive textiles inspired by cephalopod-skin.[187] To control IR emission/transmission, both types of textiles function with mechanical actions such as flipping the textile or applying/releasing strain. Zhang *et al.* demonstrated a self-adaptive radiative cooling/heating textile that reacts to humidity (or ambient temperature).[188] The authors used hydrophilic–hydrophobic side-by-side metafibers, leading to differential expansion in different RH conditions. This causes mechanical actuation of the metafibers within the

knitted fabric, achieving dynamic tunable IR gating in clothing (Fig. 10f). This side-by-side structure is composed of carbon nanotube-coated triacetate-cellulose (Fig. 10g). The inter-fiber distances in the textiles instantaneously varies in response to humidity changes (Fig. 10h). In higher humidity conditions, more water is absorbed by the hydrophilic cellulose, which swell more than the hydrophobic triacetate side. This is a key mechanism to actuate the spacing between metafibers in response to changes in humidity. At high humidity levels, the interfiber distance increases by $\sim$100 μm, leading to an 'open' state, while the opposite takes place at a low humidity level (*i.e.*, 'close' state). In the 'open' state, not only radiative cooling is enhanced, but convective and evaporative cooling are also synergically increased through the open area. This IR gating effect was quantified using IR transmittance variation as a function of humidity. As shown in Fig. 10i, the IR transmittance changes with the same tendency as RH.

4. Perspectives

Following decades of research, the field of radiative cooling is quickly approaching performance limits. For instance, reflectivity in the solar spectral range and thermal emissivity in the NIR-FIR region has already reached unity.[13] Furthermore, deep-subfreezing by as much as 60 °C from ambient temperatures have been reported in an earlier stage of the research.[189] While these achievements hold potential, obstacles remain in the field of radiative cooling: (1) over-cooling at night or winter, (2) feasibility for real-world applications, and (3) fundamental challenges pertaining to passive radiative cooling.

For year-round thermoregulation, automatically switchable radiative thermostats should be developed. Continued effort has recently resulted in self-adaptive radiative thermostats for clothing and buildings using PCMs with photonic approaches and humidity-sensitive metafibers. W-doped VO_2 operates at the practical transition temperature of $\sim$25 °C. The TARC with W-doped VO_2 demonstrates temperature-adaptive radiative cooling depending on the ambient temperature. In addition to such a self-adaptive film, VO_2 has also been implemented in a smart window which features thermoregulation by modulating emissivity in the LWIR region at ambient temperatures. In addition to buildings, dynamically tunable IR gating textiles can thermally regulate personal temperature for comfort. These novel textiles are composed of metafibers with hydrophilic-hydrophobic features in a single fiber. These contradicting properties cause the variable swelling of the fiber depending on humidity or air temperature, resulting in self-adaptive IR gating clothing. Although the effectiveness of these self-adaptive radiative thermostats was demonstrated, they are proof-of-concept and not fully optimized in terms of spectral features, operating temperatures, and production-cost. Therefore, future research should endeavor to develop advanced photonic strategies with PCMs that minimize solar absorption and can transition at lower temperatures. In addition, developing smart textiles that not only modulate IR-transmittance, but regulate absorption/reflection in the solar spectrum should be prioritized.

The second challenge primarily concerns fabrication and industry-level application. The fabrication process must be cost-effective, large-scaled, and not time consuming. Cooling paint[190] and fabric[11] that reached the 100 m^2 scale have been reported and a bilayer design has been suggested to effectively obtain high reflectivity in both the Vis. and UV regions.[191] However, materials that achieve sufficient durability and reasonable cost are yet to be demonstrated. Available integration area and visible appeal are remaining challenges from an economic perspective. Because the radiative cooler can only be adopted in a detached manner, such as the top floor of a building, complicated solar cell systems, and small sized wearable devices, the installation area is always limited. Because the radiative cooling power is proportional to the exposed surface area,[17] a sufficiently large installation site must be secured to obtain the desired cooling performance. Therefore, the tradeoff between cooling capacity resulting from installation area and downsizing the cooling system should carefully be considered. Visual discomfort caused by highly reflective surfaces is an important issue for the widespread adoption of radiative cooling technologies. As a vital area of research efforts, many studies on colored radiative coolers have been performed by considering aesthetic aspects of building exteriors.[16,191,192] However, more advanced photonic approaches are required to overcome the hurdle of fully reflecting most solar irradiation except for minimal absorption that is necessary for coloration.[193,194]

There are fundamental limitations in the field of passive radiative cooling, including inherit performance limit and dependency on season and region. Passive cooling potential has been evaluated to be maximally $\sim$150 W m^{-2},[190] which is only $\sim$35% of the average total cooling power in buildings.[13] Thus, the performance of active cooling cannot be achieved even with optimal radiative cooling capacity. It is, therefore, proposed to combine existing active cooling systems with passive radiative cooling as efficient hybrid systems, not to completely replace them. Minimizing non-radiative heat loss (*i.e.*, convection and conduction) is also one of the ways to maximize radiative cooling capacity. Furthermore, because the performance of radiative cooling is highly dependent on local atmospheric constituents (primarily water), it is crucial to take this into account to design radiative coolers that are appropriate for different climates. From a modeling perspective, the design of a radiative cooling material typically involves various programs employing optical problem solvers including Maxwell equations and finite-difference time-domain method (FDTD),[12] customized codes for iterative processes,[195] as well as programs for simulating varying weather conditions.[196] However, there are major drawbacks in using various software packages. To maximize the cooling effect, it is necessary to precisely tailor the emission spectrum of the radiative cooler. Some researchers have tried to solve this problem using machine learning.[197,198] However, the demand for huge data sets and high initial costs are a barrier to entry.

Therefore, there remain exceedingly complicated challenges to the field of radiative cooling. To address these, yet-to-be developed materials might offer unprecedented mechanical

strength and resistance to soiling while being scalable and low cost. Multidisciplinary studies are highly recommended, not only to take advantage of the existing knowledge bases, but also to stimulate the imagination to solve these uncertain challenges.

5. Summary

Only ten years ago, radiative cooling was a limited technology that could only operate at night due to undesired solar absorption. However, the rapid development of photonic metamaterials completely reversed this situation,[199–205] realizing daytime radiative cooling. The advanced photonic strategies offered routes to simultaneously achieve near-unity solar reflection and selective or broadband thermal emission. Following the early stage of this technology, which pursued the development of daytime radiative coolers, interest shifted to scalable and affordable radiative coolers for building-exterior materials, which is the domain that could benefit the most from radiative cooling. These efforts have resulted in radiative coolers in the

Table 1 A brief summary the material, structure, cooling performance, and application of experimentally demonstrated daytime radiative cooler

Material and structure	Cooling performance (other performance)	Experiment condition	Application	Year	Ref.
Seven layers of HfO_2 and SiO_2	4.9 °C below ambient air temperature and cooling power of 40.1 W m^{-2}	850 W m^{-2} average solar irradiance	Building exterior	2014	Raman *et al.*[9]
50 mm-thick polymer–glass bead hybrid organic–inorganic film and a 200 nm-thick Ag thin film layers	Cool water to 10.6 °C below ambient and an average cooling power of 607 W m^{-2} at noon (12–2 p.m.)	952 W m^{-2} average solar irradiance at 26.5 L (h m^2)$^{-1}$ volumetric flow rate	Water-based radiative cooling for building	2019	Zhao *et al.*[57]
Five alternating layers of a-Si:H and SiO_2 multilayers coated with 50 μm-thick poly-dimethylsiloxane (PDMS) layer	Average 5.2 °C temperature reduction of an inner temperature compares to the transparent selective emitter that transmits most of the incoming solar irradiance under direct sunlight	550 W m^{-2} of peak solar irradiance	Enclosure	2021	Kim *et al.*[81]
4 μm of PDMS layer, 100 nm of Ag layer, and 500 μm-thick micro-patterned quartz layer coated with 10 μm of PDMS from top to bottom	Lowered the temperature of a radiative object inside an enclosure by an average 4 °C compared to a conventional radiative cooler, which is composed of an aluminum plate coated with ~100 μm thick PDMS	810 W m^{-2} average solar power and average humidity of ~44%.	Enclosure	2020	Heo *et al.*[17]
Nano polyethylene (PE)	2.7 and 2 °C lower skin temperature when covered with nanoPE cloth and with processed nanoPE cloth than when covered with cotton	Skin simulator	Textile	2016	Hsu *et al.*[11]
PTFE/TiO_2 embedded PLA fibers	5, 6.8, 7, 5.8, and 10.2 °C lower than that of the cotton, spandex, chiffon, linen, and bare skin simulator	~620 W m^{-2} of peak solar irradiance	Textile	2021	Zeng *et al.*[107]
Porous SEBS	~7 °C cooling than non-porous SEBS covered skin	~840 W m^{-2} of peak solar irradiance	Wearable devices	2020	Xu *et al.*[127]
Porous PMMA/SEBS bi-layer	~7 °C cooling than black elastomer covered skin after 7 min exposure to sunlight	~820 W m^{-2} of average solar intensity and 18 °C of ambient temperature	Wearable devices	2021	Kang *et al.*[128]
Two dimensional SIO_2 micro grating	Average 6 °C cooling, leading to absolute increase of 2% in open-circuit voltage for InGaP/GaAs/Ge multi-junction solar cell	989 W m^{-2} of peak solar intensity and a clear sky	Solar cell	2021	Heo *et al.*[147]
Soda-lime glass wafer	Achieving 5 °C to 36 °C temperature drop and an 8% to 27% relative increase of open-circuit voltage for a GaSb solar cell	5 to 6 W of average heat load on the solar cell	Solar cell	2020	Wang *et al.*[31]
A glass-polymer hybrid film	Output voltage of ~40 mV cm^{-2} and an output power of ~10 nW cm^{-2}	~500 W m^{-2} of solar irradiance and ~25 °C of ambient temperature	TEG	2021	Ren *et al.*[159]
Black paint coated aluminum disk	Cooling 4–5 °C under ambient air (cold side), experimentally 25 mW m^{-2} of power generation	Nighttime outdoor condition	TEG	2019	Raman *et al.*[21]
The structure consists of layers of PDMS and Ag on an aluminum (Al) substrate, with a thickness of 100 μm, 150 nm, and 1 mm	(Condensation rate) below 10 °C of ambient temperature and condensing ~8.5 mL per day	800 W m^{-2} of peak solar intensity and all the devices were tilted ~15° toward the west to reduce absorption of solar radiation	Dew harvesting	2021	Zhou *et al.*[14]
A multi-layer of PDMS 100 μm on 500 μm of glass substrate. The backside of the substrate is coated with 140 nm of Ag and 1 nm of chromium	(Condensation rate) 52 g m^{-2} h^{-1} of dew mass flux is obtained over a period of nearly 3 h	200 W m^{-2} of solar irradiance and at a mean RH of 96% in August	Dew harvesting	2021	Haechler *et al.*[171]
$W_xV_{1-x}O_2$/BaF_2 2D grating on Ag	Emissivity from 0.2 for ambient temperatures lower than 15 °C to 0.90 for temperature above 30 °C	Under direct solar irradiance	Self-adaptive radiative thermostat	2021	Tang *et al.*[75]
VO_2/PMMA/Low E coated glass	Emissivity from 0.21 to 0.61 at transition temperature of 60 °C	Indoor experiment	Self-adaptive radiative thermostat	2021	Wang *et al.*[74]

form of, *e.g.*, rigid plates,[206,207] flexible films[208,209]/polymers,[210,211] paints,[212,213] and woods.[13]

In this paper, we reviewed the fundamental principles, materials, and structures of the radiative coolers. The various applications in these studies are divided into three main classes according to the targeted situation: large-scale facilities, personal thermal management, energy harvesting, dew harvesting, and radiative self-adaptation as summarized in Table 1. Buildings, stationary vehicles, and greenhouses are large-scale enclosures that account for a large portion of global energy consumptions, making passive radiative cooling a promising complement to traditional cooling systems. Great progress has also been made in personal thermal management. Clothing that utilizes radiative cooling is very effective for personal thermal management and can further contribute to indoor cooling energy-savings. Because human skin is a near-blackbody in the LWIR region, radiative cooling clothes are adapted for IR-transparency and solar opacity. NanoPE textiles serve as a core material to achieve this objective. The size and weight of wearable devices have continuously become smaller and lighter. However, using convection and conduction to cool them have limitations. Furthermore, because these devices incorporate wireless communication technologies, a metallic heat sink cannot be used to dissipate the heat from the device. Therefore, non-metallic/flexible radiative coolers are promising avenues for the heat management of wearable devices. In particular, advanced wearable devices, which pursue multi-functionality and high operating speed, may suffer from self-heating issues. Several studies have also demonstrated the integration of radiative cooling with energy generation devices, such as solar cells and TEGs. Elevated temperature reduces the efficiency and lifetime of solar cells. Passive radiative cooling is a cost-effective cooling technology owing to its simple and lightweight nature. The combination of TEGs and radiative coolers facilitates the all-day electricity generation. A radiatively cooled surface increases the temperature difference between hot and cold sides in TEG, therefore enhancing the Seebeck effect underpinning TEG. The electricity generation by radiative cooler-combined TEG can fulfill the nighttime imbalance of PV cells. Moreover, power generation and personal thermal management can be simultaneously achieved by integrating TEG with radiative cooling textiles, enabling control of device thermal management and supplying energy to operate it. Water scarcity is increasingly considered as an unavoidable global risk. With the emergence of a new class of thermal emitter, the radiative cooler can provide daytime passive water harvesting. A radiative cooler has its optimal condition in terms of shape, hydrophilic properties, and infrared emittance. Recent innovations have offered effective designs to maximize dew yield.

In summary, pioneering studies on photonic metamaterials have laid the foundation for the realization of daytime radiative cooling. Material engineering approaches enables implementation of radiative coolers in various forms with affordability and scalability. In addition, self-adaptive radiative thermostats have also recently been developed owing to technical/academic progress. There are remaining challenges in terms of spectral features and cost, however, the overall progress in radiative cooling/heating technologies can alleviate energy consumption, which is a significant contribution to the global effort for achieving 'Net-zero emissions'. Although this review is by no means exhaustive, we hope that it provides a stimulating introduction to novices and experts alike.

Author contributions

Se-Yeon Heo: writing, conceptualization, visualization, data curation, writing – review and editing. Gil Ju Lee: supervision, conceptualization, visualization, writing – review and editing, investigation. Young Min Song: supervision, project administration, writing – review and editing, investigation.

Conflicts of interest

There are no conflicts to declare.

Acknowledgements

This work was supported by the National Research Foundation of Korea (NRF-2021R1C1C2013605/2020R1A2C2004983/2018M3D1-A1058997/2017M3D1A1039288/2021R1A4A2001827 and by the GIST Research Institute (GRI) grant funded by the GIST in 2022. This work was also supported by Pusan National University Research Grant, 2021.

References

1 X. Yin, R. Yang, G. Tan and S. Fan, *Science*, 2020, **370**, 786–791.
2 K. Y. Kondrat'Yev, *Radiative heat exchange in the atmosphere*, Elsevier, 2013.
3 S. Catalanotti, V. Cuomo, G. Piro, D. Ruggi, V. Silvestrini and G. Troise, *Sol. Energy*, 1975, **17**, 83–89.
4 T. Eriksson and C. Granqvist, *Appl. Opt.*, 1982, **21**, 4381–4388.
5 F. Arago, *Reprinted in Oeuvres Complè, tes de Francois Arago*, 1828, **8**, 87.
6 N. N. Shi, C.-C. Tsai, F. Camino, G. D. Bernard, N. Yu and R. Wehner, *Science*, 2015, **349**, 298–301.
7 D. Xie, Z. Yang, X. Liu, S. Cui, H. Zhou and T. Fan, *Soft Matter*, 2019, **15**, 4294–4300.
8 M. M. Hossain and M. Gu, *Adv. Sci.*, 2016, **3**, 1500360.
9 A. P. Raman, M. Abou Anoma, L. Zhu, E. Rephaeli and S. Fan, *Nature*, 2014, **515**, 540–544.
10 M. M. Hossain, B. Jia and M. Gu, *Adv. Opt. Mater.*, 2015, **3**, 1047–1051.
11 P.-C. Hsu, A. Y. Song, P. B. Catrysse, C. Liu, Y. Peng, J. Xie, S. Fan and Y. Cui, *Science*, 2016, **353**, 1019–1023.
12 Y. Zhai, Y. Ma, S. N. David, D. Zhao, R. Lou, G. Tan, R. Yang and X. Yin, *Science*, 2017, **355**, 1062–1066.
13 T. Li, Y. Zhai, S. He, W. Gan, Z. Wei, M. Heidarinejad, D. Dalgo, R. Mi, X. Zhao and J. Song, *Science*, 2019, **364**, 760–763.

14 M. Zhou, H. Song, X. Xu, A. Shahsafi, Y. Qu, Z. Xia, Z. Ma, M. A. Kats, J. Zhu and B. S. Ooi, *Proc. Natl. Acad. Sci. U. S. A.*, 2021, **118**, e2019292118.
15 D. Zhao, A. Aili, Y. Zhai, S. Xu, G. Tan, X. Yin and R. Yang, *Appl. Phys. Rev.*, 2019, **6**, 021306.
16 G. J. Lee, Y. J. Kim, H. M. Kim, Y. J. Yoo and Y. M. Song, *Adv. Opt. Mater.*, 2018, **6**, 1800707.
17 S.-Y. Heo, G. J. Lee, Y. J. Kim, S. Ishii, M. S. Kim, T. J. Seok, B. J. Lee, H. Lee and Y. M. Song, *Sci. Adv.*, 2020, **6**, eabb1906.
18 J. Alleman and J. Brophy,*Social Studies Excursions, K-3. Book One: Powerful Units on Food, Clothing, and Shelter*, ERIC, 2001.
19 Y. Xu, B. Sun, Y. Ling, Q. Fei, Z. Chen, X. Li, P. Guo, N. Jeon, S. Goswami and Y. Liao, *Proc. Natl. Acad. Sci. U. S. A.*, 2020, **117**, 205–213.
20 W. Li, Y. Shi, K. Chen, L. Zhu and S. Fan, *ACS Photonics*, 2017, **4**, 774–782.
21 A. P. Raman, W. Li and S. H. Fan, *Joule*, 2019, **3**, 2679–2686.
22 S. Fan and W. Li, *Nat. Photonics*, 2022, 1–9.
23 W. Li and S. Fan, *Opt. Photon. News*, 2019, **30**, 32–39.
24 X. Sun, Y. Sun, Z. Zhou, M. A. Alam and P. Bermel, *Nanophotonics*, 2017, **6**, 997–1015.
25 M. Zeyghami, D. Y. Goswami and E. Stefanakos, *Sol. Energy Mater. Sol. Cells*, 2018, **178**, 115–128.
26 **www.radi-cool.co.jp**.
27 **www.skycoolsystems.com**.
28 **www.metare.net**.
29 **www.solcold.co**.
30 **www.foel.cool**.
31 Z. Wang, D. Kortge, J. Zhu, Z. Zhou, H. Torsina, C. Lee and P. Bermel, *Joule*, 2020, **4**, 2702–2717.
32 X. Yu, J. Chan and C. Chen, *Nano Energy*, 2021, 106259.
33 L. Zhu, A. P. Raman and S. Fan, *Proc. Natl. Acad. Sci. U. S. A.*, 2015, **112**, 12282–12287.
34 D. Shen, C. Yu and W. Wang, *Appl. Therm. Eng.*, 2020, **176**, 115479.
35 C. Y. Tso, K. C. Chan and C. Y. Chao, *Renewable Energy*, 2017, **106**, 52–61.
36 D. Lee, M. Go, S. Son, M. Kim, T. Badloe, H. Lee, J. K. Kim and J. Rho, *Nano Energy*, 2021, **79**, 105426.
37 L. Zhou, H. Song, J. Liang, M. Singer, M. Zhou, E. Stegenburgs, N. Zhang, C. Xu, T. Ng and Z. Yu, *Nat. Sustainability*, 2019, **2**, 718–724.
38 M. Ma, K. Zhang, L. Chen and S. Tang, *Build. Services Eng. Res. Technol.*, 2021, **42**, 26–44.
39 D. Zhao, A. Aili, X. Yin, G. Tan and R. Yang, *Energy Build.*, 2019, **203**, 109453.
40 J. Mandal, S. Mandal, J. Brewer, A. Ramachandran and A. P. Raman, 2020, arXiv preprint arXiv:2006.11931.
41 X. Lu, P. Xu, H. Wang, T. Yang and J. Hou, *Renewable Sustainable Energy Rev.*, 2016, **65**, 1079–1097.
42 B. Givoni, *Energy Build.*, 1977, **1**, 141–145.
43 G. B. Smith, A. R. Gentle, M. D. Arnold, M. A. Gali and M. B. Cortie, *Renewable Energy Environ. Sustainability*, 2017, **2**, 13.
44 M. Muselli, *Energy Build.*, 2010, **42**, 945–954.
45 A. R. Gentle and G. B. Smith, *Adv. Sci.*, 2015, **2**, 1500119.
46 R. Yang and X. Yin, *Nature Sustainability*, 2019, **2**, 663–664.
47 G. Sastry, First radiant cooled commercial building in India – critical analysis of energy, comfort and cost, *World energy engineering congress (WEEC) 2012*, Atlanta, 2012, pp. 1474–1479.
48 J. Chen and L. Lu, *Sol. Energy*, 2020, **212**, 125–151.
49 Z. Liu, H. Tan and G. Ma, *Int. J. Ventil.*, 2017, **16**, 255–267.
50 F. S. E. Center and D. Parker, Florida Solar Energy Center, 2008, **https://stars.library.ucf.edu/fsec/396**.
51 S. Ito and N. Miura, *J. Sol. Energy Eng.*, 1989, **111**, 251–256.
52 B. Zhao, M. Hu, X. Ao, N. Chen and G. Pei, *Appl. Energy*, 2019, **236**, 489–513.
53 Z. Li, Q. Chen, Y. Song, B. Zhu and J. Zhu, *Adv. Mater. Technol.*, 2020, **5**, 1901007.
54 D. Pearlmutter and P. Berliner, *Energy Build.*, 2017, **144**, 295–302.
55 S. N. Kharrufa and Y. Adil, *Build. Environ.*, 2008, **43**, 82–89.
56 M. Sodha, U. Singh, A. Srivastava and G. Tiwari, *Build. Environ.*, 1981, **16**, 93–98.
57 D. Zhao, A. Aili, Y. Zhai, J. Lu, D. Kidd, G. Tan, X. Yin and R. Yang, *Joule*, 2019, **3**, 111–123.
58 K. Zhao, X.-H. Liu and Y. Jiang, *Renewable Sustainable Energy Rev.*, 2016, **55**, 1083–1096.
59 Y. Man, H. Yang, J. D. Spitler and Z. Fang, *Appl. Energy*, 2011, **88**, 4160–4171.
60 M. Matsuta, S. Terada and H. Ito, *Sol. Energy*, 1987, **39**, 183–186.
61 M. F. Farahani, G. Heidarinejad and S. Delfani, *Energy Build.*, 2010, **42**, 2131–2138.
62 K. Zhang, D. Zhao, X. Yin, R. Yang and G. Tan, *Appl. Energy*, 2018, **224**, 371–381.
63 E. A. Goldstein, A. P. Raman and S. Fan, *Nat. Energy*, 2017, **2**, 1–7.
64 M. Hu, G. Pei, Q. Wang, J. Li, Y. Wang and J. Ji, *Appl. Energy*, 2016, **179**, 899–908.
65 M. Hu, B. Zhao, X. Ao, Y. Su, Y. Wang and G. Pei, *Energy*, 2018, **155**, 360–369.
66 M. Hu, G. Pei, L. Li, R. Zheng, J. Li and J. Ji, *Int. J. Photoenergy*, 2015, **2**, 1–9.
67 C. Yong, W. Yiping and Z. Li, *Renewable Energy*, 2015, **74**, 627–632.
68 S. Yoon, M. Kim, J. Seo, S. Kim, H. Lee, J. Lee and B. J. Lee, *Energy Build.*, 2021, **241**, 110921.
69 U. Eicker and A. Dalibard, *Sol. Energy*, 2011, **85**, 1322–1335.
70 M. Hu, B. Zhao, J. Li, Y. Wang and G. Pei, *Energy*, 2017, **137**, 419–430.
71 B. Zhao, M. Hu, X. Ao, Q. Xuan and G. Pei, *Sol. Energy Mater. Sol. Cells*, 2018, **178**, 266–272.
72 B. Zhao, M. Hu, X. Ao and G. Pei, *Appl. Energy*, 2017, **205**, 626–634.
73 S. Zhang and J. Niu, *Energy Build.*, 2012, **54**, 122–130.
74 S. C. Wang, T. Y. Jiang, Y. Meng, R. G. Yang, G. Tan and Y. Long, *Science*, 2021, **374**, 1501–1504.

75 K. C. Tang, K. C. Dong, J. C. Li, M. P. Gordon, F. G. Reichertz, H. Kim, Y. Rho, Q. J. Wang, C. Y. Lin, C. P. Grigoropoulos, A. Javey, J. J. Urban, J. Yao, R. Levinson and J. Q. Wu, *Science*, 2021, **374**, 1504–1509.
76 M. W. Liddament, *Indoor Air*, 2000, **10**, 193–199.
77 B. Yu, Z. Hu, M. Liu, H. Yang, Q. Kong and Y. Liu, *Int. J. Refrig.*, 2009, **32**, 3–20.
78 M. Hu, B. Zhao, X. Ao, P. Zhao, Y. Su and G. Pei, *Appl. Energy*, 2018, **231**, 288–300.
79 A. Grundstein, V. Meentemeyer and J. Dowd, *Int. J. Biometeorol.*, 2009, **53**, 255–261.
80 H. F. Krous, J. M. Nadeau, R. I. Fukumoto, B. D. Blackbourne and R. W. Byard, *Am. J. Forensic Med. Pathol.*, 2001, **22**, 374–382.
81 M. Kim, D. Lee, S. Son, Y. Yang, H. Lee and J. Rho, *Adv. Opt. Mater.*, 2021, 2002226.
82 D. H. Kim, G. J. Lee, S.-Y. Heo, I.-S. Kang and Y. M. Song, *Sol. Energy Mater. Sol. Cells*, 2021, **230**, 111173.
83 X. Liu, C. Xiao, P. Wang, M. Yan, H. Wang, P. Xie, G. Liu, H. Zhou, D. Zhang and T. Fan, *Adv. Opt. Mater.*, 2021, **9**, 2101151.
84 W. Baudoin, A. Nersisyan, A. Shamilov, A. Hodder, D. Gutierrez, D. Pascale, S. S. Nicola, N. Gruda, L. Urban and J. Tanny, *FAO*, 2017, 230.
85 P. V. Nelson, *Greenhouse operation and management*, Prentice Hall, 1991.
86 L. Shen, R. Lou, Y. Park, Y. Guo, E. J. Stallknecht, Y. Xiao, D. Rieder, R. Yang, E. S. Runkle and X. Yin, *Nat. Food*, 2021, **2**, 434–441.
87 J.-W. Cho, S.-K. Chang, S.-J. Park, S. Oh, Y. Nam and S.-K. Kim, *Curr. Appl. Phys.*, 2020, **20**, 1073–1079.
88 P. C. Hsu and X. Q. Li, *Science*, 2020, **370**, 784–785.
89 L. L. Cai, A. Y. Song, W. Li, P. C. Hsu, D. C. Lin, P. B. Catrysse, Y. Y. Liu, Y. C. Peng, J. Chen, H. X. Wang, J. W. Xu, A. K. Yang, S. H. Fan and Y. Cui, *Adv. Mater.*, 2018, **30**, 1802152.
90 G. Kim, K. Park, K. J. Hwang and S. H. Jin, *ACS Nano*, 2021, **15**, 15962–15971.
91 T. T. Gao, Z. Yang, C. J. Chen, Y. J. Li, K. Fu, J. Q. Dai, E. M. Hitz, H. Xie, B. Y. Liu, J. W. Song, B. Yang and L. B. Hu, *ACS Nano*, 2017, **11**, 11513–11520.
92 D. Li, X. Liu, W. Li, Z. Lin, B. Zhu, Z. Li, J. Li, B. Li, S. Fan and J. Xie, *Nat. Nanotechnol.*, 2021, **16**, 153–158.
93 N. N. Shi, C.-C. Tsai, M. J. Carter, J. Mandal, A. C. Overvig, M. Y. Sfeir, M. Lu, C. L. Craig, G. D. Bernard and Y. Yang, *Light: Sci. Appl.*, 2018, **7**, 1–9.
94 B. Zhu, W. Li, Q. Zhang, D. Li, X. Liu, Y. Wang, N. Xu, Z. Wu, J. Li and X. Li, *Nat. Nanotechnol.*, 2021, **16**, 1342–1348.
95 J. Li, Y. Liang, W. Li, N. Xu, B. Zhu, Z. Wu, X. Wang, S. Fan, M. Wang and J. Zhu, *Sci. Adv.*, 2022, **8**, eabj9756.
96 L. L. Cai, Y. C. Peng, J. W. Xu, C. Y. Zhou, C. X. Zhou, P. L. Wu, D. C. Lin, S. H. Fan and Y. Cui, *Joule*, 2019, **3**, 1478–1486.
97 H. Luo, Q. Li, K. K. Du, Z. Q. Xu, H. Z. Zhu, D. L. Liu, L. Cai, P. Ghosh and M. Qiu, *Nano Energy*, 2019, **65**, 103998.
98 S. M. Jeong, J. Ahn, Y. K. Choi, T. Lim, K. Seo, T. Hong, G. H. Choi, H. Kim, B. W. Lee, S. Y. Park and S. Ju, *NPG Asia Mater.*, 2020, **12**, 32.
99 X. Li, Y. Yang, Z. Quan, L. Wang, D. Ji, F. Li, X. Qin, J. Yu and S. Ramakrishna, *Chem. Eng. J.*, 2022, **430**, 133093.
100 L. L. Cai, A. Y. Song, P. L. Wu, P. C. Hsu, Y. C. Peng, J. Chen, C. Liu, P. B. Catrysse, Y. Y. Liu, A. K. Yang, C. X. Zhou, C. Y. Zhou, S. H. Fan and Y. Cui, *Nat. Commun.*, 2017, **8**, 496.
101 J. W. Wu, R. Hu, S. N. Zeng, W. Xi, S. Y. Huang, J. H. Deng and G. M. Tao, *ACS Appl. Mater. Interfaces*, 2020, **12**, 19015–19022.
102 Y. J. Yoo, J. H. Lim, G. J. Lee, K. I. Jang and Y. M. Song, *Nanoscale*, 2017, **9**, 2986–2991.
103 Z. Q. Wang, H. W. Yang, Y. Li and X. H. Zheng, *ACS Appl. Mater. Interfaces*, 2020, **12**, 15726–15736.
104 P. C. Hsu, X. G. Liu, C. Liu, X. Xie, H. R. Lee, A. J. Welch, T. Zhao and Y. Cui, *Nano Lett.*, 2015, **15**, 365–371.
105 Y. C. Peng, J. Chen, A. Y. Song, P. B. Catrysse, P. C. Hsu, L. L. Cai, B. F. Liu, Y. Y. Zhu, G. M. Zhou, D. S. Wu, H. R. Lee, S. H. Fan and Y. Cui, *Nat. Sustainability*, 2018, **1**, 105–112.
106 M. Alberghini, S. Hong, L. M. Lozano, V. Korolovych, Y. Huang, F. Signorato, S. H. Zandavi, C. Fucetola, I. Uluturk, M. Y. Tolstorukov, G. Chen, P. Asinari, R. M. Osgood, M. Fasano and S. V. Boriskina, *Nat. Sustainability*, 2021, **4**, 715.
107 S. N. Zeng, S. J. Pian, M. Y. Su, Z. N. Wang, M. Q. Wu, X. H. Liu, M. Y. Chen, Y. Z. Xiang, J. W. Wu, M. N. Zhang, Q. Q. Cen, Y. W. Tang, X. H. Zhou, Z. H. Huang, R. Wang, A. Tunuhe, X. Y. Sun, Z. G. Xia, M. W. Tian, M. Chen, X. Ma, L. Yang, J. Zhou, H. M. Zhou, Q. Yang, X. Li, Y. G. Ma and G. M. Tao, *Science*, 2021, **373**, 692–696.
108 W. Gao, S. Emaminejad, H. Y. Y. Nyein, S. Challa, K. Chen, A. Peck, H. M. Fahad, H. Ota, H. Shiraki and D. J. N. Kiriya, *Nature*, 2016, **529**, 509–514.
109 D. Shen, M. Xiao, G. Zou, L. Liu, W. W. Duley and Y. N. J. A. M. Zhou, *Adv. Mater.*, 2018, **30**, 1705925.
110 X. Xu, J. Chen, S. Cai, Z. Long, Y. Zhang, L. Su, S. He, C. Tang, P. Liu and H. J. A. M. Peng, *Adv. Mater.*, 2018, **30**, 1803165.
111 H. Zhang, P. Gutruf, K. Meacham, M. C. Montana, X. Zhao, A. M. Chiarelli, A. Vázquez-Guardado, A. Norris, L. Lu and Q. J. S. a Guo, *Sci. Adv.*, 2019, **5**, eaaw0873.
112 H. U. Chung, B. H. Kim, J. Y. Lee, J. Lee, Z. Xie, E. M. Ibler, K. Lee, A. Banks, J. Y. Jeong and J. J. S. Kim, *Science*, 2019, **363**, eaau0780.
113 K.-I. Jang, S. Y. Han, S. Xu, K. E. Mathewson, Y. Zhang, J.-W. Jeong, G.-T. Kim, R. C. Webb, J. W. Lee and T. J. J. N. C. Dawidczyk, *Nat. Commun.*, 2014, **5**, 1–10.
114 S. Choi, S. I. Han, D. Jung, H. J. Hwang, C. Lim, S. Bae, O. K. Park, C. M. Tschabrunn, M. Lee and S. Y. J. N. N. Bae, *Nat. Nanotechnol.*, 2018, **13**, 1048–1056.
115 S.-H. Byun, J. Y. Sim, Z. Zhou, J. Lee, R. Qazi, M. C. Walicki, K. E. Parker, M. P. Haney, S. H. Choi and A. J. S. A. Shon, *Sci. Adv.*, 2019, **5**, eaay0418.

116 D.-H. Kim, N. Lu, R. Ghaffari, Y.-S. Kim, S. P. Lee, L. Xu, J. Wu, R.-H. Kim, J. Song and Z. J. N. M. Liu, *Nat. Mater.*, 2011, **10**, 316–323.
117 H. Kim, Y. S. Kim, M. Mahmood, S. Kwon, N. Zavanelli, H. S. Kim, Y. S. Rim, F. Epps and W. H. J. A. S. Yeo, *Adv. Sci.*, 2020, **7**, 2000810.
118 Y. Ino, M. Nakashima, T. Morita, Y. Hori, H. Kishikawa, N. Hagiwara, T. Matsutani, T. Nomura and A. J. J. C. R. Sakamoto, *JA Clin. Rep.*, 2018, **4**, 1–2.
119 K. G. Murphy, J. A. Secunda and M. A. J. A. Rockoff, *Anesthesiology*, 1990, **73**, 350–352.
120 T.-i Kim, J. G. McCall, Y. H. Jung, X. Huang, E. R. Siuda, Y. Li, J. Song, Y. M. Song, H. A. Pao and R.-H. J. S. Kim, *Science*, 2013, **340**, 211–216.
121 I. Heinonen, R. M. Brothers, J. Kemppainen, J. Knuuti, K. K. Kalliokoski and C. G. J. J. O. A. P. Crandall, *J. Appl. Physiol.*, 2011, **111**, 818–824.
122 R. Clarke, R. Hellon and A. J. T. J. O. P. Lind, *J. Physiol.*, 1958, **143**, 454–473.
123 R. Edwards, R. Harris, E. Hultman, L. Kaijser, D. Koh and L. J. T. J. O. P. Nordesjö, *J. Physiol.*, 1972, **220**, 335–352.
124 K. Vinogradova, L. Nikulina, S. Braslavskii, E. Solovieva, K. Mynbaev, V. Nikolaev, A. Romanov and V. J. M. P. Bougrov, *Mater. Phys. Mech.*, 2013, **18**, 143–147.
125 M. Vázquez, N. Núñez, E. Nogueira and A. J. M. R. Borreguero, *Microelectron. Reliab.*, 2010, **50**, 1559–1562.
126 T.-i Kim, S. Hyun Lee, Y. Li, Y. Shi, G. Shin, S. Dan Lee, Y. Huang, J. A. Rogers and J. J. A. P. L. Su Yu, *Appl. Phys. Lett.*, 2014, **104**, 051901.
127 Y. D. Xu, B. H. Sun, Y. Ling, Q. H. Fei, Z. Y. Chen, X. P. Li, P. J. Guo, N. Jeon, S. Goswami, Y. X. Liao, S. H. Ding, Q. S. Yu, J. Lin, G. L. Huang and Z. Yan, *Proc. Natl. Acad. Sci. U. S. A.*, 2020, **117**, 205–213.
128 M. H. Kang, G. J. Lee, J. H. Lee, M. S. Kim, Z. Yan, J. W. Jeong, K. I. Jang and Y. M. Song, *Adv. Sci.*, 2021, **8**, 2004885.
129 Y. Shi, C. Wang, Y. Yin, Y. Li, Y. Xing and J. J. A. F. M. Song, *Adv. Funct. Mater.*, 2019, **29**, 1905470.
130 H. H. Jung, J. Song, S. Nie, H. N. Jung, M. S. Kim, J. W. Jeong, Y. M. Song, J. Song and K. I. J. A. M. T. Jang, *Adv. Mater. Technol.*, 2018, **3**, 1800159.
131 W. Li, S. Buddhiraju and S. Fan, *Light: Sci. Appl.*, 2020, **9**, 1–11.
132 S. J. Byrnes, R. Blanchard and F. Capasso, *Proc. Natl. Acad. Sci. U. S. A.*, 2014, **111**, 3927–3932.
133 S. Buddhiraju, P. Santhanam and S. Fan, *Proc. Natl. Acad. Sci. U. S. A.*, 2018, **115**, E3609–E3615.
134 M. Ono, P. Santhanam, W. Li, B. Zhao and S. Fan, *Appl. Phys. Lett.*, 2019, **114**, 161102.
135 W. Shockley, *J. Appl. Phys.*, 1961, **32**, 510–519.
136 S. Chander, A. Purohit, A. Sharma, S. Nehra and M. Dhaka, *Energy Rep.*, 2015, **1**, 104–109.
137 G. F. Russell, Uniform surface temperature heat pipe and method of using the same, *US Pat.*, 4320246, 1982.
138 H. Teo, P. Lee and M. Hawlader, *Appl. Energy*, 2012, **90**, 309–315.
139 E. Cuce and P. M. Cuce, *Int. J. Ambient Energy*, 2014, **35**, 193–199.
140 S. Odeh and M. Behnia, *Heat Transfer Eng.*, 2009, **30**, 499–505.
141 M. Huang, P. Eames and B. Norton, *Sol. Energy*, 2006, **80**, 1121–1130.
142 C. Solanki, C. Sangani, D. Gunashekar and G. Antony, *Sol. Energy Mater. Sol. Cells*, 2008, **92**, 1634–1638.
143 K. Yang and C. Zuo, *Energy Convers. Manage.*, 2015, **89**, 214–221.
144 A. K. Goyal and A. Kumar, *J. Nanophoton.*, 2020, **14**, 030901.
145 S. Dou, H. Xu, J. Zhao, K. Zhang, N. Li, Y. Lin, L. Pan and Y. Li, *Adv. Mater.*, 2020, 2000697.
146 G. Perrakis, A. C. Tasolamprou, G. Kenanakis, E. N. Economou, S. Tzortzakis and M. Kafesaki, *Sci. Rep.*, 2021, **11**, 1–10.
147 S. Y. Heo, D. H. Kim, Y. M. Song and G. J. Lee, *Adv. Energy Mater.*, 2021, 2103258.
148 Y. Lu, Z. Chen, L. Ai, X. Zhang, J. Zhang, J. Li, W. Wang, R. Tan, N. Dai and W. Song, *Sol. RRL*, 2017, **1**, 1700084.
149 S. Lin, L. Ai, J. Zhang, T. Bu, H. Li, F. Huang, J. Zhang, Y. Lu and W. Song, *Sol. Energy Mater. Sol. Cells*, 2019, **203**, 110135.
150 T. S. Safi and J. N. Munday, *Opt. Express*, 2015, **23**, A1120–A1128.
151 Y. Sun, Z. Zhou, X. Jin, X. Sun, M. A. Alam and P. Bermel, *Proc. SPIE*, 2017, **10369**, 103690D.
152 Z. Zhou, Z. Wang and P. Bermel, *Opt. Express*, 2019, **27**, A404–A418.
153 J. Liu, Y. Zhang, D. Zhang, S. Jiao, Z. Zhang and Z. J. E. C. Zhou, *Energy Convers. Manage.*, 2020, **216**, 112923.
154 Z. Xia, Z. Zhang, Z. Meng, L. Ding and Z. J. A. A. M. Yu, *ACS Appl. Mater. Interfaces*, 2019, **11**, 33941–33945.
155 J. Liu, J. Zhang, J. Yuan, D. Zhang, J. Xing, Z. J. S. E. M. Zhou and S. Cells, *Sol. Energy Mater. Sol. Cells*, 2021, **220**, 110855.
156 B. Zhao, G. Pei and A. P. J. A. P. L. Raman, *Appl. Phys. Lett.*, 2020, **117**, 163903.
157 Y. Liu, S. Hou, X. Wang, L. Yin, Z. Wu, X. Wang, J. Mao, J. Sui, X. Liu and Q. J. S. Zhang, *Small*, 2022, 2106875.
158 S. Ishii, T. D. Dao and T. Nagao, *Appl. Phys. Lett.*, 2020, **117**, 013901.
159 W. Ren, Y. Sun, D. L. Zhao, A. Aili, S. Zhang, C. Q. Shi, J. L. Zhang, H. Y. Geng, J. Zhang, L. X. Zhang, J. L. Xiao and R. G. Yang, *Sci. Adv.*, 2021, **7**, abe0586.
160 S. Khan, J. Kim, K. Roh, G. Park and W. Kim, *Nano Energy*, 2021, **87**, 106180.
161 S. Hong, Y. Gu, J. K. Seo, J. Wang, P. Liu, Y. S. Meng, S. Xu and R. K. Chen, *Sci. Adv.*, 2019, **5**, eaaw0536.
162 Y. Tu, R. Wang, Y. Zhang and J. Wang, *Joule*, 2018, **2**, 1452–1475.
163 H. Jarimi, R. Powell and S. Riffat, *Int. J. Low-Carbon Technol.*, 2020, **15**, 253–276.
164 M. Tomaszkiewicz, M. Abou Najm, D. Beysens, I. Alameddine and M. El-Fadel, *Environ. Rev.*, 2015, **23**, 425–442.
165 J. Monteith, *Q. J. R. Meteorol. Soc.*, 1957, **83**, 322–341.
166 I. Gindel, *Nature*, 1965, **207**, 1173–1175.

167 B. Khalil, J. Adamowski, A. Shabbir, C. Jang, M. Rojas, K. Reilly and B. Ozga-Zielinski, *Sustainable Water Resour. Manage.*, 2016, **2**, 71–86.
168 I. Lekouch, K. Lekouch, M. Muselli, A. Mongruel, B. Kabbachi and D. Beysens, *J. Hydrol.*, 2012, **448**, 60–72.
169 M. Muselli, D. Beysens, M. Mileta and I. Milimouk, *Atmos. Res.*, 2009, **92**, 455–463.
170 M. Dong, Z. Zhang, Y. Shi, X. Zhao, S. Fan and Z. Chen, *Nanoscale Microscale Thermophys. Eng.*, 2020, **24**, 43–52.
171 I. Haechler, H. Park, G. Schnoering, T. Gulich, M. Rohner, A. Tripathy, A. Milionis, T. M. Schutzius and D. Poulikakos, *Sci. Adv.*, 2021, **7**, eabf3978.
172 M. Chen, Z. Yi, S. Tao, S. Wang, Z. Fang, C. Lu and Z. Xu, *Global Challenges*, 2020, **4**, 1900094.
173 W. Li, M. Dong, L. Fan, J. J. John, Z. Chen and S. Fan, *ACS Photonics*, 2020, **8**, 269–275.
174 U. E. I. Administration, 2020, **https://www.eia.gov/totalenergy/data/annual/**.
175 U. E. I. Administration, 2015, **https://www.eia.gov/consumption/residential/**.
176 W. J. M. Kort-Kamp, S. Kramadhati, A. K. Azad, M. T. Reiten and D. A. R. Dalvit, *ACS Photon.*, 2018, **5**, 4554–4560.
177 M. Ono, K. F. Chen, W. Li and S. H. Fan, *Opt. Express*, 2018, **26**, A777–A787.
178 X. Zhao, S. A. Mofid, B. P. Jelle, G. Tan, X. Yin and R. Yang, *Appl. Energy*, 2020, **278**, 115663.
179 K.-K. Du, Q. Li, Y.-B. Lyu, J.-C. Ding, Y. Lu, Z.-Y. Cheng and M. Qiu, *Light: Sci. Appl.*, 2017, **6**, e16194.
180 X. Zhao, S. A. Mofid, T. Gao, G. Tan, B. P. Jelle, X. Yin and R. Yang, *Mater. Today Phys.*, 2020, **13**, 100205.
181 H. Zhu, Q. Li, C. Zheng, Y. Hong, Z. Xu, H. Wang, W. Shen, S. Kaur, P. Ghosh and M. Qiu, *Light: Sci. Appl.*, 2020, **9**, 1–8.
182 S. Lee, K. Hippalgaonkar, F. Yang, J. Hong, C. Ko, J. Suh, K. Liu, K. Wang, J. J. Urban and X. J. S. Zhang, *Science*, 2017, **355**, 371–374.
183 P. C. Hsu, C. Liu, A. Y. Song, Z. Zhang, Y. C. Peng, J. Xie, K. Liu, C. L. Wu, P. B. Catrysse, L. L. Cai, S. Zhai, A. Majumdar, S. H. Fan and Y. Cui, *Sci. Adv.*, 2017, **3**, e1700895.
184 H. Luo, Y. N. Zhu, Z. Q. Xu, Y. Hong, P. T. Ghosh, S. Kaur, M. B. Wu, C. Y. Yang, M. Qiu and Q. Li, *Nano Lett.*, 2021, **21**, 3879–3886.
185 X. Li, B. Ma, J. Dai, C. Sui, D. Pande, D. R. Smith, L. C. Brinson and P.-C. Hsu, *Sci. Adv.*, 2021, **7**, eabj7906.
186 H. Luo, Q. Li, C. Zheng, Y. Hong, Z. Xu, H. Wang, W. Shen, S. Kaur, P. Ghosh and M. Qiu, *Light: Sci. Appl.*, 2020, **9**, 60.
187 E. M. Leung, M. C. Escobar, G. T. Stiubianu, S. R. Jim, A. L. Vyatskikh, Z. J. Feng, N. Garner, P. Patel, K. L. Naughton, M. Follador, E. Karshalev, M. D. Trexler and A. A. Gorodetsky, *Nat. Commun.*, 2019, **10**, 1947.
188 X. A. Zhang, S. J. Yu, B. B. Xu, M. Li, Z. W. Peng, Y. X. Wang, S. L. Deng, X. J. Wu, Z. P. Wu, M. Ouyang and Y. H. Wang, *Science*, 2019, **363**, 619–623.
189 Z. Chen, L. Zhu, A. Raman and S. Fan, *Nat. Commun.*, 2016, **7**, 1–5.
190 J. Mandal, Y. Yang, N. Yu and A. P. Raman, *Joule*, 2020, **4**, 1350–1356.
191 Y. Chen, J. Mandal, W. Li, A. Smith-Washington, C.-C. Tsai, W. Huang, S. Shrestha, N. Yu, R. P. Han and A. Cao, *Sci. Adv.*, 2020, **6**, eaaz5413.
192 W. Li, Y. Shi, Z. Chen and S. Fan, *Nat. Commun.*, 2018, **9**, 1–8.
193 S. Son, S. Jeon, D. Chae, S. Y. Lee, Y. Liu, H. Lim, S. J. Oh and H. Lee, *Nano Energy*, 2021, **79**, 105461.
194 S. Min, S. Jeon, K. Yun and J. Shin, *ACS Photonics*, 2022, **9**, 1196–1205.
195 Z. F. Mira, S.-Y. Heo, G. J. Lee and Y. M. Song, *J. Quant. Spectrosc. Radiat. Transfer*, 2021, 107774.
196 C. Liu, Y. Wu, B. Wang, C. Zhao and H. Bao, *Sol. Energy*, 2019, **183**, 218–225.
197 H. Zhang, J. Huang, D. Fan and P. Tie, *Opt. Mater. Express*, 2021, **11**, 3706–3716.
198 J. J. García-Esteban, J. Bravo-Abad and J. C. Cuevas, *Phys. Rev. Appl.*, 2021, **16**, 064006.
199 X. Liu, T. Tyler, T. Starr, A. F. Starr, N. M. Jokerst and W. J. Padilla, *Phys. Rev. Lett.*, 2011, **107**, 045901.
200 M. De Zoysa, T. Asano, K. Mochizuki, A. Oskooi, T. Inoue and S. Noda, *Nat. Photonics*, 2012, **6**, 535–539.
201 E. Rephaeli, A. Raman and S. Fan, *Nano Lett.*, 2013, **13**, 1457–1461.
202 P. N. Dyachenko, S. Molesky, A. Y. Petrov, M. Störmer, T. Krekeler, S. Lang, M. Ritter, Z. Jacob and M. Eich, *Nat. Commun.*, 2016, **7**, 1–8.
203 W. Li and S. Fan, *Opt. Express*, 2018, **26**, 15995–16021.
204 J. Xu, J. Mandal and A. P. Raman, *Science*, 2021, **372**, 393–397.
205 D. Lee, S. So, G. Hu, M. Kim, T. Badloe, H. Cho, J. Kim, H. Kim, C.-W. Qiu and J. Rho, *eLight*, 2022, **2**, 1–23.
206 D. Chae, M. Kim, P.-H. Jung, S. Son, J. Seo, Y. Liu, B. J. Lee and H. Lee, *ACS Appl. Mater. Interfaces*, 2020, **12**, 8073–8081.
207 J. Seo, M. Choi, J. Lee and B. J. Lee, *J. Quant. Spectrosc. Radiat. Transfer*, 2022, **284**, 108165.
208 J. Peoples, Y.-W. Hung, X. Li, D. Gallagher, N. Fruehe, M. Pottschmidt, C. Breseman, C. Adams, A. Yuksel and J. Braun, *Appl. Energy*, 2022, **310**, 118368.
209 T. Y. Yoon, S. Son, S. Min, D. Chae, H. Y. Woo, J.-Y. Chae, H. Lim, J. Shin, T. Paik and H. Lee, *Mater. Today Phys.*, 2021, **21**, 100510.
210 A. Aili, Z. Wei, Y. Chen, D. Zhao, R. Yang and X. Yin, *Mater. Today Phys.*, 2019, **10**, 100127.
211 K. Herrmann, T. Lauster, Q. Song and M. Retsch, *Advanced Energy and Sustainability Research*, 2022, **3**, 2100166.
212 X. Li, J. Peoples, P. Yao and X. Ruan, *ACS Appl. Mater. Interfaces*, 2021, **13**, 21733–21739.
213 D. Chae, S. Son, H. Lim, P.-H. Jung, J. Ha and H. Lee, *Mater. Today Phys.*, 2021, **18**, 100389.